A MEASURE OF STABILITY FOR MOBILE MANIPULATORS WITH APPLICATION TO HEAVY-DUTY HYDRAULIC MACHINES

by

Ahmad Ghasempoor-Nobandgany

A thesis
presented to the University of Manitoba
in fulfilment of the
thesis requirement for the degree of
Master of Science
in
Mechanical Engineering

Winnipeg, Manitoba, Canada 1994

ISBN 0-315-99110-0

Name ___

Dissertation Abstracts International is arranged by broad, general subject categories. Please select the one subject which most nearly describes the content of your dissertation. Enter the corresponding four-digit code in the spaces provided.

Mechanical Engineering — SUBJECT TERM

0548 — SUBJECT CODE

U·M·I

Subject Categories

THE HUMANITIES AND SOCIAL SCIENCES

COMMUNICATIONS AND THE ARTS
Architecture 0729
Art History 0377
Cinema 0900
Dance 0378
Fine Arts 0357
Information Science 0723
Journalism 0391
Library Science 0399
Mass Communications 0708
Music 0413
Speech Communication 0459
Theater 0465

EDUCATION
General 0515
Administration 0514
Adult and Continuing 0516
Agricultural 0517
Art 0273
Bilingual and Multicultural 0282
Business 0688
Community College 0275
Curriculum and Instruction 0727
Early Childhood 0518
Elementary 0524
Finance 0277
Guidance and Counseling 0519
Health 0680
Higher 0745
History of 0520
Home Economics 0278
Industrial 0521
Language and Literature 0279
Mathematics 0280
Music 0522
Philosophy of 0998
Physical 0523
Psychology 0525
Reading 0535
Religious 0527
Sciences 0714
Secondary 0533
Social Sciences 0534
Sociology of 0340
Special 0529
Teacher Training 0530
Technology 0710
Tests and Measurements 0288
Vocational 0747

LANGUAGE, LITERATURE AND LINGUISTICS
Language
- General 0679
- Ancient 0289
- Linguistics 0290
- Modern 0291

Literature
- General 0401
- Classical 0294
- Comparative 0295
- Medieval 0297
- Modern 0298
- African 0316
- American 0591
- Asian 0305
- Canadian (English) 0352
- Canadian (French) 0355
- English 0593
- Germanic 0311
- Latin American 0312
- Middle Eastern 0315
- Romance 0313
- Slavic and East European 0314

PHILOSOPHY, RELIGION AND THEOLOGY
Philosophy 0422
Religion
- General 0318
- Biblical Studies 0321
- Clergy 0319
- History of 0320
- Philosophy of 0322

Theology 0469

SOCIAL SCIENCES
American Studies 0323
Anthropology
- Archaeology 0324
- Cultural 0326
- Physical 0327

Business Administration
- General 0310
- Accounting 0272
- Banking 0770
- Management 0454
- Marketing 0338

Canadian Studies 0385
Economics
- General 0501
- Agricultural 0503
- Commerce-Business 0505
- Finance 0508
- History 0509
- Labor 0510
- Theory 0511

Folklore 0358
Geography 0366
Gerontology 0351
History
- General 0578
- Ancient 0579
- Medieval 0581
- Modern 0582
- Black 0328
- African 0331
- Asia, Australia and Oceania 0332
- Canadian 0334
- European 0335
- Latin American 0336
- Middle Eastern 0333
- United States 0337

History of Science 0585
Law 0398
Political Science
- General 0615
- International Law and Relations 0616
- Public Administration 0617

Recreation 0814
Social Work 0452
Sociology
- General 0626
- Criminology and Penology 0627
- Demography 0938
- Ethnic and Racial Studies 0631
- Individual and Family Studies 0628
- Industrial and Labor Relations 0629
- Public and Social Welfare 0630
- Social Structure and Development 0700
- Theory and Methods 0344

Transportation 0709
Urban and Regional Planning 0999
Women's Studies 0453

THE SCIENCES AND ENGINEERING

BIOLOGICAL SCIENCES
Agriculture
- General 0473
- Agronomy 0285
- Animal Culture and Nutrition 0475
- Animal Pathology 0476
- Food Science and Technology 0359
- Forestry and Wildlife 0478
- Plant Culture 0479
- Plant Pathology 0480
- Plant Physiology 0817
- Range Management 0777
- Wood Technology 0746

Biology
- General 0306
- Anatomy 0287
- Biostatistics 0308
- Botany 0309
- Cell 0379
- Ecology 0329
- Entomology 0353
- Genetics 0369
- Limnology 0793
- Microbiology 0410
- Molecular 0307
- Neuroscience 0317
- Oceanography 0416
- Physiology 0433
- Radiation 0821
- Veterinary Science 0778
- Zoology 0472

Biophysics
- General 0786
- Medical 0760

EARTH SCIENCES
Biogeochemistry 0425
Geochemistry 0996
Geodesy 0370
Geology 0372
Geophysics 0373
Hydrology 0388
Mineralogy 0411
Paleobotany 0345
Paleoecology 0426
Paleontology 0418
Paleozoology 0985
Palynology 0427
Physical Geography 0368
Physical Oceanography 0415

HEALTH AND ENVIRONMENTAL SCIENCES
Environmental Sciences 0768
Health Sciences
- General 0566
- Audiology 0300
- Chemotherapy 0992
- Dentistry 0567
- Education 0350
- Hospital Management 0769
- Human Development 0758
- Immunology 0982
- Medicine and Surgery 0564
- Mental Health 0347
- Nursing 0569
- Nutrition 0570
- Obstetrics and Gynecology 0380
- Occupational Health and Therapy 0354
- Ophthalmology 0381
- Pathology 0571
- Pharmacology 0419
- Pharmacy 0572
- Physical Therapy 0382
- Public Health 0573
- Radiology 0574
- Recreation 0575
- Speech Pathology 0460
- Toxicology 0383

Home Economics 0386

PHYSICAL SCIENCES

Pure Sciences
Chemistry
- General 0485
- Agricultural 0749
- Analytical 0486
- Biochemistry 0487
- Inorganic 0488
- Nuclear 0738
- Organic 0490
- Pharmaceutical 0491
- Physical 0494
- Polymer 0495
- Radiation 0754

Mathematics 0405
Physics
- General 0605
- Acoustics 0986
- Astronomy and Astrophysics 0606
- Atmospheric Science 0608
- Atomic 0748
- Electronics and Electricity 0607
- Elementary Particles and High Energy 0798
- Fluid and Plasma 0759
- Molecular 0609
- Nuclear 0610
- Optics 0752
- Radiation 0756
- Solid State 0611

Statistics 0463

Applied Sciences
Applied Mechanics 0346
Computer Science 0984
Engineering
- General 0537
- Aerospace 0538
- Agricultural 0539
- Automotive 0540
- Biomedical 0541
- Chemical 0542
- Civil 0543
- Electronics and Electrical 0544
- Heat and Thermodynamics 0348
- Hydraulic 0545
- Industrial 0546
- Marine 0547
- Materials Science 0794
- Mechanical 0548
- Metallurgy 0743
- Mining 0551
- Nuclear 0552
- Packaging 0549
- Petroleum 0765
- Sanitary and Municipal 0554
- System Science 0790

Geotechnology 0428
Operations Research 0796
Plastics Technology 0795
Textile Technology 0994

PSYCHOLOGY
General 0621
Behavioral 0384
Clinical 0622
Developmental 0620
Experimental 0623
Industrial 0624
Personality 0625
Physiological 0989
Psychobiology 0349
Psychometrics 0632
Social 0451

A MEASURE OF STABILITY FOR MOBILE MANIPULATORS WITH APPLICATION TO HEAVY-DUTY HYDRAULIC MACHINES

BY

AHMAD GHASEMPOOR-NOBANDGANY

A Thesis submitted to the Faculty of Graduate Studies of the University of Manitoba in partial fulfillment of the requirements for the degree of

MASTER OF SCIENCE

Abstract

Many machines that are used in forest, mining and construction industries, are mobile, heavy-duty and carry hydraulically-actuated manipulators. They constantly interact with unstructured environments and experience different loading. As a result, these machines are susceptible to tipping-over. This thesis is concerned with the development of a suitable algorithm for computing the margin of stability of such mobile manipulators in real-time. The margin of stability shows the proximity of the machine to tipping-over condition at each instant.

The stability analysis algorithm developed in this thesis is an extension of the method by Messuri and Klien (1985) and is able to quantitatively reflect the effect of all relevant factors on the machine stability. These factors include the location of the centre of gravity, spatially placed contact points with ground, presence of substantial forces and moments arising from the manipulation of the implement, and rough terrain condition. The algorithm first determines the instantaneous unstable configuration about each axis of potential overturning of the machine. A new concept called 'equilibrium plane' is defined for this purpose. When the machine is hypothetically rotated around the edge until the center of gravity falls in this plane, the net moment around the edge becomes minimum in the absolute sense. The amount of the work necessary to bring the machine from the current stable position to this verge of instability is then computed to determine the margin of stability.

The methodology and algorithm developed in this thesis is exemplified with an excavator-based log loader. The algorithm is implemented in a simulation program written in C language and real-time aspect of it is studied. Simulation studies of the candidate machine clearly show that the forces and moments arising from the manipulation of the implement are important in stability status and thus cannot be overlooked. Furthermore, a simple two-dimensional graphical display format is proposed for quantitative demonstration (to the machine operator) of the proximity to instability at each instant.

تقدیم به پدر و مادرم ؛

به پاس فداکاریها و مهربانیهای بیشمارشان ،

و تقدیم به همسرم ؛

به پاس عشق و همراهیش .

Acknowledgment

The author would like to express deep gratitude and appreciation to his thesis advisor, Dr. N. Sepehri, for suggesting the thesis topic and for his constant guidance, encouragement and support.

The author would also like to thank Dr. D. Strong and Dr. S. Onyshko, members of his examining committee, for their valuable suggestions and corrections in the course of preparation of this thesis.

This work could have not been completed without the unconditional love and support of my wife Maryam.

Contents

List of Tables

List of Figures

List of Symbols

$\mathbf{S}$	Static stability
$\mathbf{H}$	Walking height
m	Mass
g	Acceleration of gravity
$\vec{\mathbf{F}}$	Force vector
$\vec{\mathbf{M}}$	Moment vector
h	Pitch
$\vec{\mathbf{v}}$	Linear velocity vector
P	Power
K	Normalized virtual power
$\mathbf{XYZ}$	Machin coordinate frame
$\bar{\mathbf{X}}\bar{\mathbf{Y}}\bar{\mathbf{Z}}$	Gravity coordinate frame
$f_1, f_2, \ldots$	Feet contact points
x_{CG}, y_{CG}, z_{CG}	Coordinates of the centre of gravity
$\tilde{b}$	Unit vector in direction of support boundary edge
$\tilde{z}$	Unit vector in vertical direction
A	Homogeneous transformation matrix
${}^0\hat{\vec{s}}_i$	Position vector to centre of gravit of link
I	Inertia tensor

$\dot{\vec{v}}$	Linear acceleration vector
${}^{i}\vec{N}_i$	Link's reaction moment vector
${}^{i}\vec{F}_i$	Link's reaction force vector
${}^{i}\vec{f}_i$	Joint's reaction force vector
${}^{i}\vec{n}_i$	Joint's reaction moment vector
$\vec{R}_{CG}$	Position vector of the centre of gravity
$	Screw axis
θ	Joint angle angle
$\dot{\theta}$	Joint's angular velocity
$\ddot{\theta}$	Joint's angular acceleration
ϕ	Equilibrium plane angle
ϕ_x	Roll angle
ϕ_y	Pitch angle
α	Gradient angle
$\vec{\omega}$	Angular velocity vector
$\dot{\vec{\omega}}$	Angular acceleration vector

Chapter 1

Introduction

Forest, mining and construction industries use a wide variety of machines, each adapted to particular operating conditions and functions. Recently these industries have applied teleoperation concepts to improve the performance and efficiency of their machineries. In teleoperation, the operator's demands (position and velocity) are passed to a computer which is interfaced to the machine and performs the actual control. This approach has many potential benefits. For example, repetitive tasks can be performed automatically and operators can be relieved from some of the low-level decisions (equipment operation) to concentrate more on high-level decisions (task planning).

Almost all the machines that are used in such primary industries have the common characteristics that they are mobile, heavy-duty, have hydraulically-actuated manipulator-like structures (see Figure 1.1), and constantly interact with the environment. Therefore, they are susceptible to instability. Here by instability we mean the tipping-over of the machine. Although modern equipment protects the operator, accidents such as machine tipping over still results in personal injury and equipment damage [1].

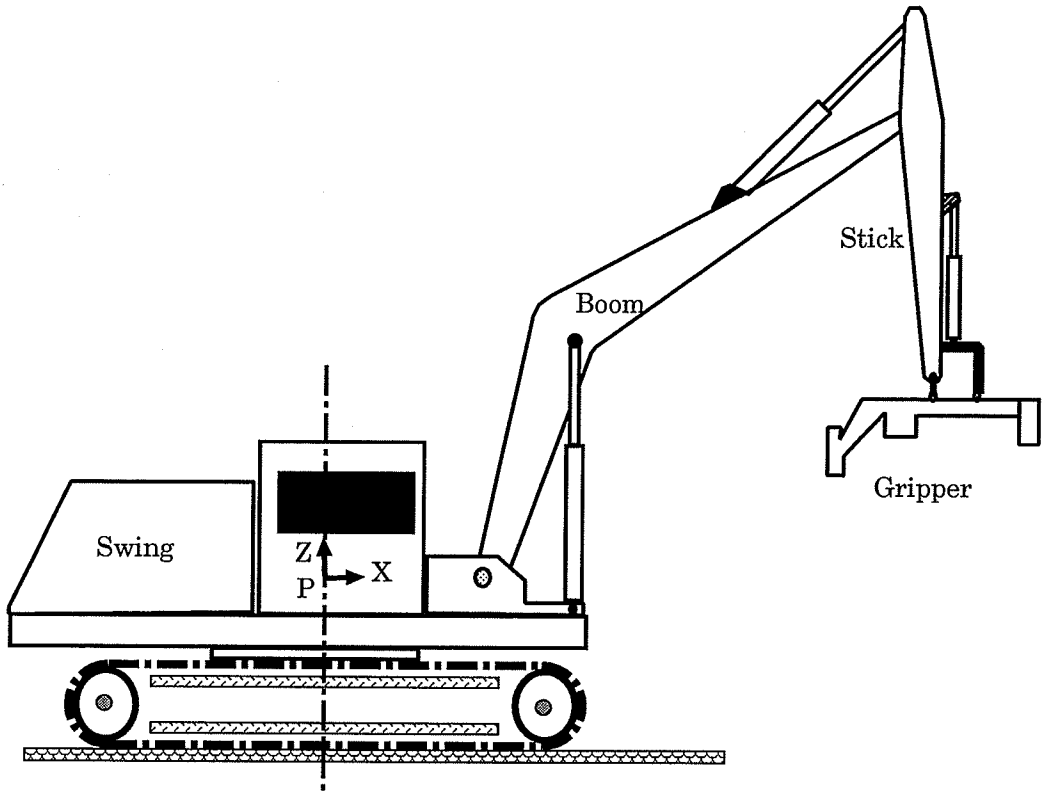

Figure 1.1: Typical mobile heavy-duty hydraulic machine.

The objective of this thesis was to first establish a scheme suitable for determining the potential of tipping over for the class of machines that are usually used in primary industries. Such a scheme can be used as part of a fault diagnostic system in order to relieve the operator from often non-intuitive and exhaustive task of maintaining the stability of the machine especially in the presence of large loadings or interaction with the environment while performing different tasks. The algorithm can also be used within a simulation program at the design level. This simulation program can provide an inexpensive, fast and safe method to fine tune the design details of different parts of the machine based on the stability criteria. One example of these design details is the amount and location of the counterweight.

Initial work on stability of mobile vehicles was only concerned with the static

stability as applied to slow moving walking machines. McGhee and Frank [2] defined a measure of stability for machines walking over an even terrain. Their work was later modified by Song and Waldron [3] to include the effect of motion over rough terrain or sloped ground. Messuri and Klein [4] introduced a different measure of stability termed "Energy Stability Margin", which could evaluate the level of stability of the machine including the effect of the vertical position of the centre of gravity [5]. Davidson and Schweitzer [6] developed a method based on screw mechanics for stability assessment which included the effect of inertial and external loads originating from the manipulator-like tool attached to the machine. These methods though valuable, have limited application to the type of machines subject to this study. The reason is that none of these methods can take into consideration all factors affecting the stability of the class of mobile heavy-duty hydraulic manipulators under investigation. These factors include the location of centre of gravity, spatially placed contact points with ground, presence of substantial inertial and external loadings and rough terrain condition.

As a part of this thesis, a new measure of stability is introduced which is in fact an extension of Messuri and Klein's method. Compared with the existing methods, the method presented in this thesis can quantitatively reflect the effect of all factors contributing to the stability status of the machine.

The thesis is organized as follows. In Chapter 2, existing measures of stability for moving base manipulators are reviewed and evaluated. In Chapter 3, a new measure of stability is introduced and a software package for real-time stability analysis of a 215B Caterpillar excavator is developed. Chapter 4 includes simulation studies of the stability characteristics of the excavator-based machine, using the algorithm developed in Chapter 3. Finally a graphical display concept which quantitatively shows the stability condition of the machine at each instant is presented in Chapter 5 which is followed by conclusions and suggestions in Chapter 6.

Chapter 2

Literature Review

Most of the work concerning the stability of vehicles has been done with static stability of legged locomotion systems in mind. However, when non-sliding contact with the ground is assumed, it doesn't make any difference whether the vehicle is legged, wheeled or a combination of both [6]. In this chapter, we first study existing measures of stability and investigate the potentials and limitations of each technique. The primary criterion for evaluating these measures is the ability to reflect the effect of all relevant factors on stability including the terrain condition, centre of gravity position and general destabilizing forces and moments applied to a vehicle. For machines used in forestry and construction industries, the destabilizing forces and moments originate from the manipulator-like arm carried by the vehicle. In this chapter, it is shown that none of the existing measures of stability fulfills the above criterion and a need for developing a new measure of stability is discussed.

2.1 Static Stability Based on Projection Method

Until recently most of the research on static stability of vehicle locomotion was based on McGhee and Frank's definitions of static stability. Studying the legged locomotion in 1968, they developed a series of definitions and theorems to determine the static stability of a walking machine while moving over an even terrain [2]. The static stability assessment criterion is established through the following definitions:

Definition 1 : The *support pattern* associated with a given support state is the minimum area convex point set in the support plane such that all of the leg contact points are contained [2].

Definition 2: An ideal legged locomotion machine is *statically stable* if all legs in contact with the support plane at the given time remain in contact with that plane when all legs of the machine are fixed at their locations, and the translational and rotational velocities of the resulting rigid body are simultaneously reduced to zero.

Definition 3: The magnitude of the *static stability margin* for an arbitrary support pattern is equal to the shortest distance from the vertical projection of the centre of gravity to any point on the boundary of the support pattern. If the pattern is statically stable, the stability margin is positive; otherwise, it is negative.

Figure 2.1 shows the application of these definitions to a case study. Here $\mathbf{S_r}$ and $\mathbf{S_f}$ are the magnitudes of the static stability measure for rear and front edges of the support boundary, respectively. Note that stability as defined by $\mathbf{S_r}$ and $\mathbf{S_f}$ are related to the moments of weight force around the sides of the support pattern. A zero restoring moment means the body is on the verge of instability. Note also that the expression for the static stability does not include the walking height $\mathbf{H}$ (centre of gravity height). $\mathbf{H}$ which is also referred to as top-heaviness, is expected to have an effect on the stability of the vehicle [4,6].

Working on the Adaptive Suspension Vehicle project at Ohio State University,

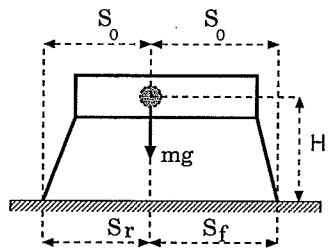

Figure 2.1: McGhee and Frank's definition of static stability margin.

Song and Waldron studied static stability of walking machines [3]. They generalized the projection method to include the case of walking over rough terrain. A rough terrain situation is when supporting feet contact points do not fall in a horizontal plane. The following definitions establish the generalized projection method for static stability assessment:

Definition 4.: A *support pattern* is a two-dimensional point set in a horizontal plane consisting of the convex hull of the vertical projection of all foot points in support phase [3].

Definition 5: The *stability margin* is the shortest distance of the vertical projection of the centre of gravity to the boundaries of the support pattern in the horizontal plane [3].

The application of these definitions for the case of a vehicle on a slope with gradient angle of θ is shown in Figure 2.2. Note that a similar condition can also occur when the vehicle is moving over a rough terrain. According to above definitions, the static stability for rear and front edges of the support boundary are [7],

$$\mathbf{S}_r = (\mathbf{S_o} - H tan\theta) cos\theta \tag{2.1}$$

$$\mathbf{S}_f = (\mathbf{S_o} + H tan\theta) cos\theta \tag{2.2}$$

Therefore the effect of moving over a rough terrain is included in this definition. The maximum gradient, θ_{max}, before the onset of instability, can be calculated by putting

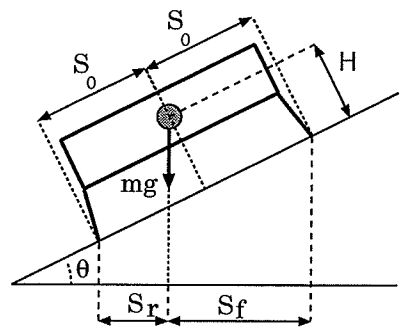

Figure 2.2: Song and Waldron measure of static stability.

$\mathbf{S}_r = 0$ and solving for θ ;

$$\theta_{max} = tan^{-1}(\frac{\mathbf{S_o}}{H}) \tag{2.3}$$

Although this definition is an improvement over McGhee and Frank's measure for static stability, it is still a qualitative measure in the sense that it cannot reflect, quantitatively, the effect of top-heaviness for all cases. For example consider the case of locomotion over a gradient with a levelled body as in Figure 2.3. Based on Song and Waldron's definition of static stability, the margin of stability is at maximum ($\mathbf{S}_r = \mathbf{S}_f = \mathbf{S_o}$). Therefore the effect of $\mathbf{H}$ is again ignored. Note also that these measures of stability predicts the same level of static stability for front and rear side, however, it seems to be easier for the vehicle to tip-over downhill rather than uphill [4]. Another limitation of this method is that the effect of destabilizing forces and moments other than gravity cannot be included. Despite the above shortcomings, the projection method has been very useful in the gait studies of walking locomotion [8,9,10].

2.2 Energy Stability Level Concept

The measure of stabilities defined so far were not able to fully take into account the effects of uneven terrain [4]. To overcome this problem, Messuri and Klein defined a

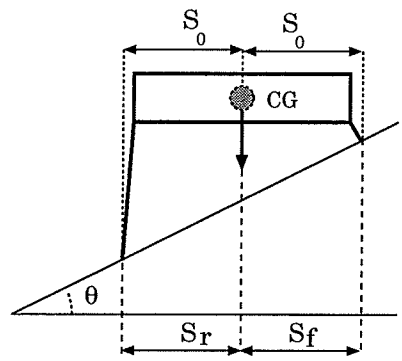

Figure 2.3: Static stability margin for levelled body on a gradient.

quantity called "Energy Stability Level" [4]. The measure of stability based on energy stability level concept is defined by the following statements:

Definition 6: The *support boundary* associated with a given support state consist of line segments connecting the tips of the support feet that form the support pattern.

Definition 7: The *energy stability level* associated with a particular edge of a support boundary is equal to the work required to rotate the body centre of gravity, about the edge, to a position where the vertical projection of the body centre of gravity lies along that edge of the support boundary.

Definition 8: The *energy stability margin* for an arbitrary support boundary is equal to the minimum of the energy stability levels associated with each edge of that support boundary.

Figure 2.4a shows the application of these definitions for the case of a vehicle with levelled body over a level terrain. Here the energy stability level is

$$E = m\,g\,h = m\,g\,Q\,(1 - cos\psi) \tag{2.4}$$

where E is the work necessary to bring the centre of gravity over the edge. Note that the centre of gravity height H is implicitly included in Equation (2.4) by the following

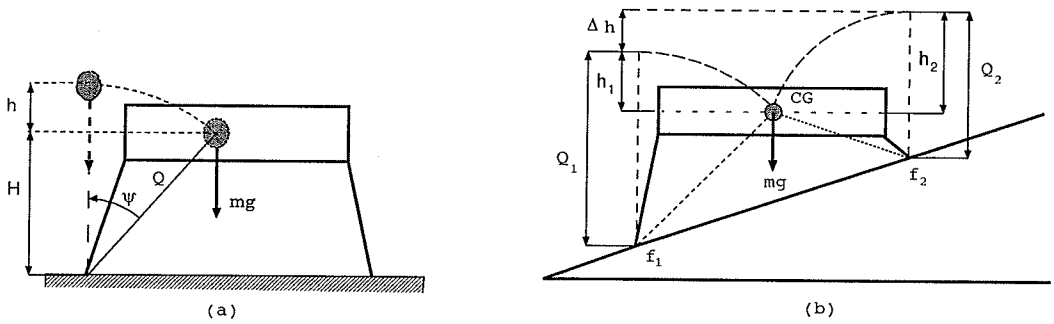

Figure 2.4: Energy stability margin.

relation,

$$\psi = cos^{-1}\frac{H}{Q} \tag{2.5}$$

Figure 2.4b shows the application of the above energy stability level concept for the case of a levelled body over a gradient. Here the energy stability level for the rear edge is mgh_1 which is less than the energy stability level for the front edge mgh_2. This shows a greater possibility of tipping over around the rear edge. Stability assessment based on the energy stability margin is therefore more accurate since there is no projection of the centre of gravity involved, and effects of top-heaviness and motion over rough terrain are also included.

The limiting gradient angle for the case of locomotion over a gradient with a fixed body height can be computed from Figure 2.5. From previous analysis, the minimum stability is associated with the rear edge. The stability level for this edge, therefore, determines the energy stability margin. ψ and θ are related such that

$$\psi = tan^{-1}(\frac{\mathbf{S_o}}{H}) - \theta \tag{2.6}$$

On the verge of instability we have $\psi = 0$, and the limiting gradient angle is obtained as,

$$\theta_{max} = tan^{-1}(\frac{\mathbf{S_o}}{H}) \tag{2.7}$$

Note that this is the same result obtained by using Song and Waldron's method. This

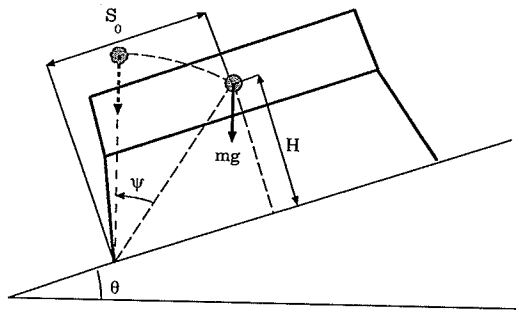

Figure 2.5: Maximum gradient using energy stability margin.

again confirms the fact that Waldron and Song's definition of stability can correctly show the onset of instability. The only drawback of the energy stability level concept is that Messuri and Klein did not include the effect of destabilizing forces and moments other than the weight force in their formulations.

2.3 Stability Measure Using Screw Mechanics

Measures of stability described so far deal with cases where the only destabilizing forces and moments are due to the weight force. In the case of heavy-duty mobile manipulators which are equipped with heavy tools, having large moment of inertia and subjected to considerable external loads, other factors come into play. In fact a large portion of destabilizing forces and moments could be due to the inertial and external loads. To incorporate these effects, Davidson and Schweitzer developed a method for stability margin calculations based on the theory of screws [6]. As this method primarily seems to provide the necessary tools for stability analysis of the machines subject to this study, a more detailed examination of it will be presented. First a brief introduction of the screw theory is presented here and in Appendix A.

Consider a rigid body with general forces $\vec{F}_1, \vec{F}_2, ...$, and general moments $\vec{M}_1, \vec{M}_2, ...$ acting simultaneously on it. We can transfer all the forces while preserving the di-

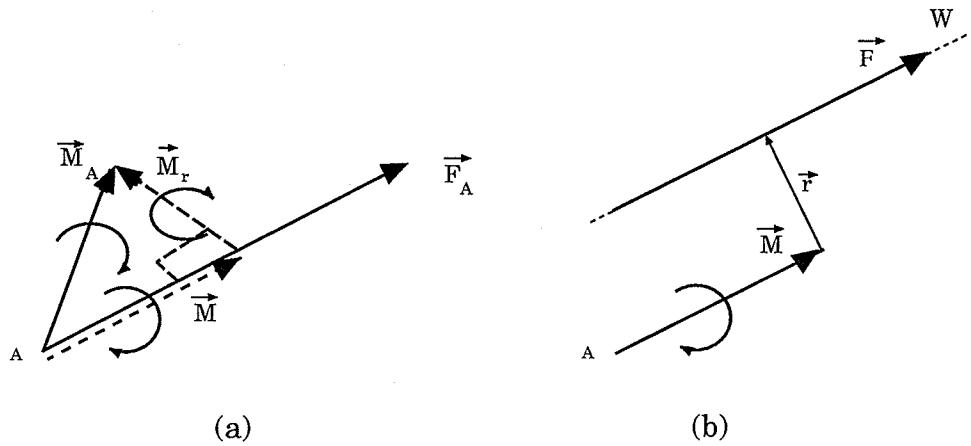

Figure 2.6: Definition of wrench.

rection of the lines of action so that they all act through an arbitrarily chosen point A. The shift to a common point produces corresponding moments $\vec{M}_{A1}, \vec{M}_{A2}, \ldots$. All the shifted force vectors $\vec{F}_{A1}, \vec{F}_{A2}, \ldots$, can be added vectorially to give the resultant force $\vec{\mathbf{F}}_A$ passing through A. Similarly all the moments both applied $\vec{M}_1, \vec{M}_2, \ldots$, and produced as a result of shifting $\vec{M}_{A1}, \vec{M}_{A2}, \ldots$, are added to give the resultant moment $\vec{\mathbf{M}}_A$ (see Figure 2.6a). In general $\vec{\mathbf{F}}_A$ and $\vec{\mathbf{M}}_A$ are not parallel. We can resolve $\vec{\mathbf{M}}_A$ in two components, $\vec{\mathbf{M}}$ parallel to $\vec{\mathbf{F}}_A$ and $\vec{\mathbf{M}}_r$ at right angle to it (see Figure 2.6a). We then shift $\vec{\mathbf{F}}_A$ by a distant $|\vec{\mathbf{r}}|$ to a line W parallel to it in the plane perpendicular to $\vec{\mathbf{M}}_r$ such that (see Figure 2.6b),

$$\vec{\mathbf{F}} \times \vec{\mathbf{r}} = -\vec{\mathbf{M}}_r \tag{2.8}$$

Line W is unique [11]. When the resultant force $\vec{\mathbf{F}}$ ($|\vec{\mathbf{F}}| = |\vec{\mathbf{F}}_A|$) lies along W, the free vector representing the corresponding resultant moment $\vec{\mathbf{M}}$ is parallel to W and therefore parallel to $\vec{\mathbf{F}}$. This force-moment combination is called a wrench, associated with the line W. It is also called a wrench-axis or a screw. A wrench has a scalar pitch h of dimension length, such that

$$h\vec{\mathbf{F}} = \vec{\mathbf{M}} \tag{2.9}$$

h is positive when the force and moment vectors are directed in the same sense according to the right-hand convention [11]. $|\vec{\mathbf{F}}|$ is called the intensity of the wrench. A concise method of representing a general wrench is provided by six Pluker line coordinates (see Appendix A for details on the Pluker coordinate system). Using the Pluker notation, a general wrench is represented by

$$|\vec{\mathbf{F}}|\$_{\mathbf{F}} = |\vec{\mathbf{F}}|[\tilde{\mathbf{a}}_{\mathbf{F}}; \vec{\mathbf{a}}_{o_{\mathbf{F}}}] \tag{2.10}$$

where $\$_{\mathbf{F}}$ represents the screw axis W. $\tilde{\mathbf{a}}_{\mathbf{F}}$ is the unit vector in the direction of the screw axis, and $\vec{\mathbf{a}}_{o_{\mathbf{F}}}$ is the moment vector of the screw axis around the origin of the coordinates frame. A Pluker coordinate system allows to combine the force and moment parts of a wrench in one notation (note that, $|\vec{\mathbf{F}}|\tilde{\mathbf{a}}_{\mathbf{F}} = \vec{\mathbf{F}}$ and $|\vec{\mathbf{F}}|\vec{\mathbf{a}}_{o_{\mathbf{F}}} = \vec{\mathbf{M}}$).

The results for the statics of a rigid body can also be applied to instantaneous kinematics of rigid bodies. An instantaneous movement of the body can be expressed as a resultant angular velocity $\vec{\omega}$ about a unique instantaneous screw axis, together with a resultant translational velocity $\vec{\mathbf{v}}$ parallel to the instantaneous screw axis. The screw axis has a unique pitch h of dimension length, such that

$$h\vec{\omega} = \vec{\mathbf{v}} \tag{2.11}$$

This combination of linear and rotational motion is called a twist [11]. A twist has an intensity of $|\vec{\omega}|$, and using the six Pluker line coordinates, is represented as

$$|\vec{\omega}|\$_{\omega} = |\vec{\omega}|[\tilde{\mathbf{a}}_{\omega}; \vec{\mathbf{a}}_{o_{\omega}}] \tag{2.12}$$

where $\$_{\omega}$ is the screw axis.

To apply screw theory to the stability analysis of moving base manipulators, Davidson and Schweitzer treated each mode of instability as a pure rotation about the axis defined by two adjacent points of the support boundary [6]. Therefore each potential tip-over axis is represented by a virtual twist $|\vec{\omega}|\$_{\omega}$, consisting of pure rotation only (i.e., a zero pitch). Figure 2.7 shows the tip-over axes ($\$_{\omega}$) for a four

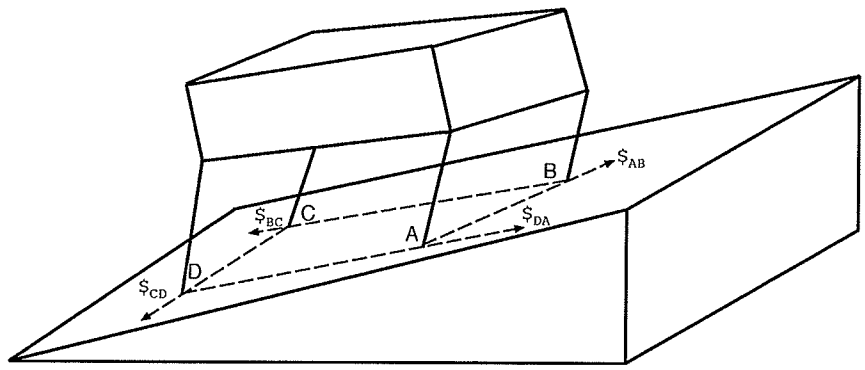

Figure 2.7: Describing potential tip-over axes using screw theory.

contact point support boundary. Similarly all forces and moments applied to the base, including gravity, inertial and external loads are represented by a wrench $|\vec{\mathbf{F}}|\$_{\mathbf{F}}$. The method calculates the virtual power produced by the action of the total wrench upon the virtual twist corresponding to each instability mode [6]. In screw theory terminology, the power P, produced by a wrench $|\vec{\mathbf{F}}|\$_{\mathbf{F}} = |\vec{\mathbf{F}}|[\tilde{\mathbf{a}}_{\mathbf{F}}; \vec{\mathbf{a}}_{o_{\mathbf{F}}}]$ acting on a twist $|\vec{\omega}|\$_{\omega} = |\vec{\omega}|[\tilde{\mathbf{a}}_{\omega}; \vec{\mathbf{a}}_{o_{\omega}}]$ is computed from (see Appendix A for details)

$$P = (\vec{\mathbf{F}} \cdot \vec{\mathbf{v}} + \vec{\omega} \cdot \vec{\mathbf{M}}) = |\vec{\mathbf{F}}||\vec{\omega}|(\tilde{\mathbf{a}}_{\mathbf{F}} \cdot \vec{\mathbf{a}}_{o_{\omega}} + \tilde{\mathbf{a}}_{\omega} \cdot \vec{\mathbf{a}}_{o_{\mathbf{F}}}) \tag{2.13}$$

which can be rewritten as,

$$P = |\vec{\mathbf{F}}||\vec{\omega}|[\$_{\omega}]^T[\Delta][\$_{\mathbf{F}}] \tag{2.14}$$

Δ is defined as

$$\Delta = \begin{bmatrix} \cdot & I_3 \\ I_3 & \cdot \end{bmatrix} \tag{2.15}$$

$[I_3]$ is a (3×3) identity matrix. Δ, in fact, performs the necessary order interchange in $\$_{\omega}$ row vector. The quantity $|\vec{\mathbf{F}}||\vec{\omega}|$ is called the power amplitude.

Davidson and Shweitzer used normalized power (i.e., with unity amplitude) and defined the normalized virtual power for each edge of the support boundary as,

$$K_{ij} = [\$_{ij}]^T[\Delta][\$_{\mathbf{F}}] \tag{2.16}$$

where subscript 'ij' refers to each tip-over axis. A negative virtual power implies stability and the magnitude of each normalized virtual power represents the level of stability for respective edge of the support boundary.

Figure 2.8 shows the application of this method to a simple case study. The body is acted upon by a concentrated force $\vec{F}$, a moment $\vec{M}$ and the weight force mg. The screw axis $\$_{12}$ for the zero-pitch twist (pure rotation) is obtained from the coordinates of two adjacent contact points (see Appendix A). These coordinates are (x_1, y_1, z_1, w_1) and (x_2, y_2, z_2, w_2) where w_1 and w_2 are homogeneous coordinates and are normally taken as unity. The coordinates of the screw axis are calculated as six (2×2) determinants from the array

$$\begin{bmatrix} w_1 & x_1 & y_1 & z_1 \\ w_2 & x_2 & y_2 & z_2 \end{bmatrix} \tag{2.17}$$

Using the formulation in Hunt [11] and assuming $z_1 = -0.5$ and $z_2 = 0.5$ we have

$$\$_{12} = [0, 0, 1, -H, l_1, 0]^T$$

Wrenches for the weight mg, force $\vec{F}$ and moment $\vec{M}$ are

$$|\vec{W}|\$_W = mg[0, -1, 0, 0, 0, 0]$$

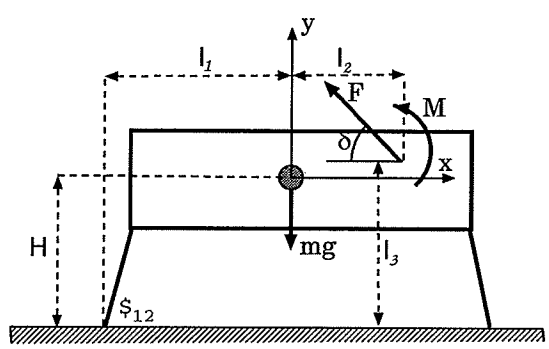

Figure 2.8: Stability analysis using screw mechanics.

$$|\vec{F}|\$_F = |F|[-cos\delta, sin\delta, 0, 0, 0, l_2 sin\delta + (l_3 - H)cos\delta]$$

$$|\vec{M}|\$_M = |M|[0, 0, 0, 0, 0, 1]$$

Therefore

$$\begin{aligned} |\vec{\mathbf{F}}|\$_{\mathbf{F}} &= |\vec{W}|\$_W + |\vec{F}|\$_F + |\vec{M}|\$_M \\ &= [-|F|cos\delta, |F|sin\delta - mg, 0, 0, 0, |M| + |F|(l_2 sin\delta + (l_3 - H)cos\delta)] \end{aligned} \tag{2.18}$$

$\$_{\mathbf{F}}$ is obtained by normalizing Equation (2.18):

$$\$_{\mathbf{F}} = [\frac{-|F|cos\delta}{norm}, \frac{|F|sin\delta - mg}{norm}, 0, 0, 0, \frac{|M| + |F|(l_2 sin\delta + (l_3 - H)cos\delta)}{norm}] \tag{2.19}$$

where

$$norm = \sqrt{(-|F|cos\delta)^2 + (|F|sin\delta - mg)^2}$$

Finally the normalized virtual power for tip-over axis $\$_{12}$ is computed from

$$\begin{aligned} K_{12} &= \begin{bmatrix} 0 & 0 & 1 & -H & l_1 & 0 \end{bmatrix} \begin{bmatrix} 0 & 0 & 0 & 1 & 0 & 0 \\ 0 & 0 & 0 & 0 & 1 & 0 \\ 0 & 0 & 0 & 0 & 0 & 1 \\ 1 & 0 & 0 & 0 & 0 & 0 \\ 0 & 1 & 0 & 0 & 0 & 0 \\ 0 & 0 & 1 & 0 & 0 & 0 \end{bmatrix} \begin{bmatrix} \frac{-|F|cos\delta}{norm} \\ \frac{|F|sin\delta - mg}{norm} \\ 0 \\ 0 \\ 0 \\ \frac{|M| + |F|(l_2 sin\delta + (l_3 - H)cos\delta)}{norm} \end{bmatrix} \\ &= \frac{l_3|F|cos\delta - l_1 mg + |F|(l_1 + l_2)sin\delta + |M|}{\sqrt{(-|F|cos\delta)^2 + (|F|sin\delta - mg)^2}} \end{aligned} \tag{2.20}$$

Note that the numerator of Equation (2.20) is in fact the summation of moments around the support boundary edge. It is seen that the walking height (centre of gravity height **H**) is absent from Equation (2.20) for K_{12}, indicating that this method can not reflect the effect of top-heaviness. In fact one can conclude that the method presented by Davidson and Shweitzer is based on computing the moment of all forces and moments acting on the vehicle around the edges of the support boundary which can impose some restrictions on the application of this method.

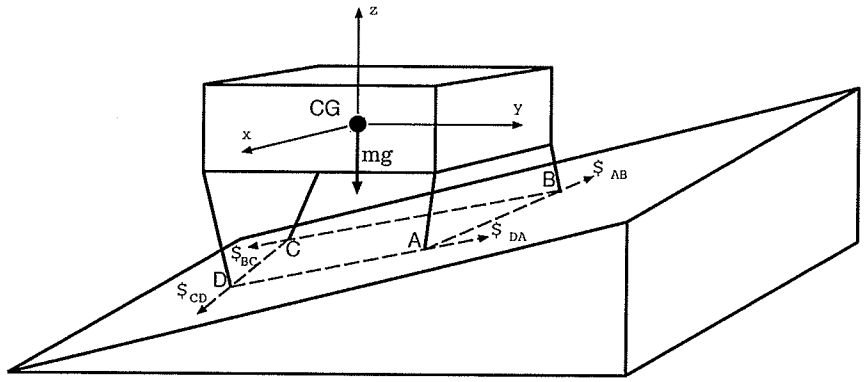

Figure 2.9: Evaluation of screw theory method.

Now consider the case of motion with levelled body over a rough terrain. Referring to Figure 2.9, the contact points have the following coordinates in xyz coordinates,

$$\begin{aligned}
(x_A, y_A, z_A, w_A) &= (1, 2, -1, 1) \\
(x_B, y_B, z_B, w_B) &= (-1, 2, -1, 1) \\
(x_C, x_C, z_C, w_C) &= (-1, -2, -2, 1) \\
(x_D, y_D, z_D, w_D) &= (1, -2, -2, 1)
\end{aligned}$$

The only acting force is assumed to be the gravity force passing through the origin of the xyz frame. Therefore we have,

$$|\vec{\mathbf{F}}|\$_{\mathbf{F}} = mg[0, 0, -1; 0, 0, 0]$$

Twist axes for sides AB and CD are,

$$\begin{aligned}
\$_{AB} &= [-1, 0, 0; 0, -1, 2]^T \\
\$_{CD} &= [1, 0, 0; 0, 2, 2]^T
\end{aligned}$$

The normalized virtual power for these two axes of potential tip-over is computed as

$$K_{AB} = \begin{bmatrix} -1 & 0 & 0 & 0 & -1 & 2 \end{bmatrix} \begin{bmatrix} 0 & 0 & 0 & 1 & 0 & 0 \\ 0 & 0 & 0 & 0 & 1 & 0 \\ 0 & 0 & 0 & 0 & 0 & 1 \\ 1 & 0 & 0 & 0 & 0 & 0 \\ 0 & 1 & 0 & 0 & 0 & 0 \\ 0 & 0 & 1 & 0 & 0 & 0 \end{bmatrix} \begin{bmatrix} 0 \\ 0 \\ -1 \\ 0 \\ 0 \\ 0 \end{bmatrix} = -2$$

$$K_{CD} = \begin{bmatrix} 1 & 0 & 0 & 0 & 2 & 2 \end{bmatrix} \begin{bmatrix} 0 & 0 & 0 & 1 & 0 & 0 \\ 0 & 0 & 0 & 0 & 1 & 0 \\ 0 & 0 & 0 & 0 & 0 & 1 \\ 1 & 0 & 0 & 0 & 0 & 0 \\ 0 & 1 & 0 & 0 & 0 & 0 \\ 0 & 0 & 1 & 0 & 0 & 0 \end{bmatrix} \begin{bmatrix} 0 \\ 0 \\ -1 \\ 0 \\ 0 \\ 0 \end{bmatrix} = -2$$

This predicts that both sides AB and CD exhibit the same level of stability which does not seem to be correct [4].

To summarize, the main advantage of this method is the ability to include destabilizing forces other than the gravity force . But we also noted some drawbacks. The method cannot reflect the effect of top-heaviness and walking over rough terrain on the stability of the body. Therefore, although this method has been found to be the only available scheme that includes external and inertial loads in the stability evaluation, it is not further studied in this thesis. A method similar to the one discussed above is presented in [12]. In this method the resultant moment around each edge of the support boundary is used as the measure of stability. This measure of stability again cannot include the effect of top-heaviness.

Chapter 3

Stability Analysis of Mobile Manipulators

The literature survey in Chapter 2, showed that the energy stability margin defined by Messuri and Klein is the only measure of stability which can include effects of top-heaviness and locomotion over rough terrain on the stability calculation of the vehicles. The method, however, is confined to stability analysis of vehicles subject to weight forces only and does not consider cases when other destabilizing forces and moments are present. The objective in this chapter is to extend the definition of energy stability level by Messuri and Klein so that it could include the effect of all possible destabilizing forces and moments. This requires the study of the contribution by external and inertial loads, to the energy stability level of a general support boundary representing spatially placed feet contacts. These loads are non-conservative in nature and have arbitrary orientations in space.

Section 3.1 is dedicated to development of an extended measure of stability which includes the effect of all relevant factors in the stability of a mobile machine. The computer software, developed for stability analysis of the class of machines subject

to this study (see Figure 1.1), is described in Section 3.2. As mentioned before these machines carry heavy-duty hydraulic manipulators and one of the contributing factors in determining the stability in these machines, is the forces and moments exerted by the manipulator-like linkage part. The algorithm presented in Section 3.2 first calculates these forces and moments, then uses the measure of stability formulated in Section 3.1 to compute their effects on the stability of the machine.

3.1 Extended Measure of Stability

3.1.1 Methodology

Figure 3.1 shows a schematic two dimensional view of a vehicle moving over a gradient. The machine is subject to gravity loading ($\mathbf{mg}$), force $\mathbf{F}$ and moment $\mathbf{M}$. Based on definitions 6,7 and 8 by Messuri and Klein, in the absence of $\mathbf{M}$ and $\mathbf{F}$, the energy stability level for the rear edge of the support boundary f_1, would be equal to $\mathrm{m}gh_1$. This is the amount of work necessary to bring the centre of gravity to a vertical plane over the rear edge. Note that since the weight is a conservative force, the work done to rotate the centre of gravity depends only on the change in the height and not the path travelled. Also note that when the centre of gravity is in the vertical plane the moment around the edge of the support boundary f_1 is zero and the body is considered to be on the verge of instability.

Now consider the case when $\mathbf{M}$ and $\mathbf{F}$ are present as shown in Figure 3.1. Intuitively, the amount of work necessary to bring the body on the verge of instability should be less since $\mathbf{M}$ and $\mathbf{F}$ are in the direction of rotation and tipping over around the rear edge appears to be easier. This observation suggests that the effect of destabilizing forces and moments should somehow be reflected in the definition of energy stability level. In this work we include such effects by calculating the amount of work

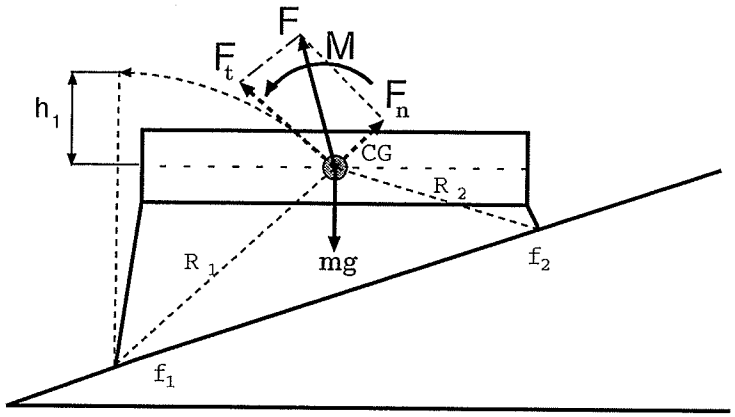

Figure 3.1: Extended measure of stability (concept).

done by these forces and moments during the hypothetical rotation of the body to the point of instability. The onset of instability occurs when the summation of all moments around the edge of a support boundary becomes zero. In the absence of **M** and **F**, this would happen when the centre of gravity is brought to a vertical plane. In the presence of **M** and **F**, the zero moment condition will be satisfied when the centre of gravity is rotated to a plane **E** (see Figure 3.2) which in general is not a vertical plane. Plane **E** is herewith called the *equilibrium plane.* The work calculations for determining the energy stability level should therefore be based on the hypothetical rotation of the body centre of gravity to the equilibrium plane. For the simple case depicted in Figure 3.2, the angle ϕ which defines the equilibrium plane **E** is obtained by putting the summation of all moments around f_1 to zero, i.e.,

$$\sum_{f_1} \mathcal{M} = F_t\, R_1 + M + m\, g\, R_1\, sin(-\phi) = 0 \tag{3.1}$$

where F_t is the component of force tangent to the circular path. The angle ϕ in this figure, is found from the following relation:

$$\phi = sin^{-1} \frac{F_t\, R_1 + M}{m\, g\, R_1} \tag{3.2}$$

Note that a destabilizing moment has been assigned a positive sign in Equation

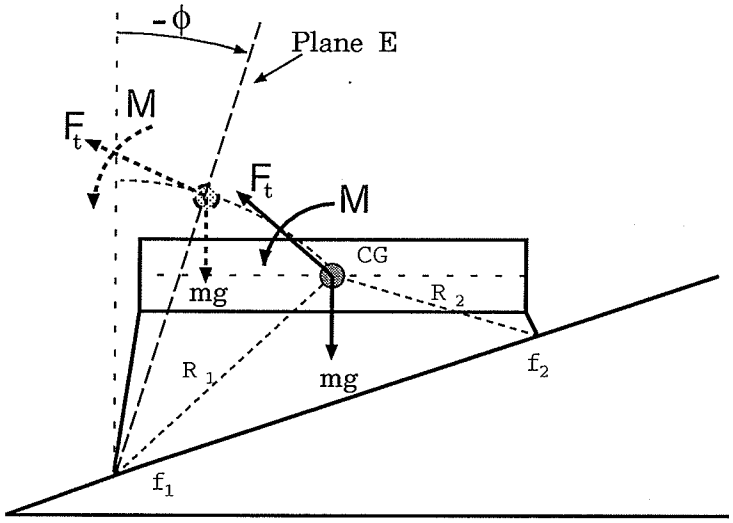

Figure 3.2: Concept of equilibrium plane.

(3.2). Equation (3.1) is constructed based on the assumption that the direction of the force F does not change relative to the body during the hypothetical rotation to the equilibrium plane.

Now consider the situation depicted in Figure 3.3. The summation of all moments around f_1 is,

$$\sum_{f_1} \mathcal{M} = m\, g\, r\, sin\phi - F\, l \tag{3.3}$$

For F> mgr/l, the sum of the moments around the point f_1 will never be zero and consequently, ϕ can not be found from Equation (3.2). This case represents a stable situation, for foot location f_1, in the sense that the body will never be on the verge of instability if rotated around this particular edge of the support boundary. However, in order to be able to include this special case in the definition of energy stability level, we simply define the equilibrium plane where the net moment around the edge of the support boundary is minimum in its absolute sense. In Figure 3.3 we note that for the case when F> mgr/l equilibrium plane is described with an angle of $\phi = 90°$ from the vertical plane.

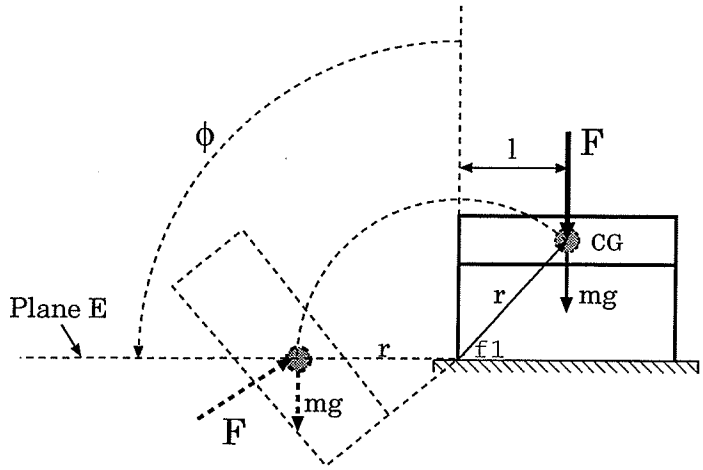

Figure 3.3: Equilibrium plane for a simple case.

Concepts presented above are now generalized for developing an extended measure of stability in following definitions. Definition of support boundary and energy stability margin here is the same as the one used by Messuri and Klein [4] (Definition 6 in Section 2.2).

Definition 9: The *equilibrium plane* associated with a particular edge of a support boundary is a plane containing the edge and with an orientation with respect to the vertical plane such that if the body is rotated around the edge until the centre of gravity falls in this plane, the net moment of all present forces and moments around the edge becomes minimum in the absolute sense.

Definition 10: The energy stability level associated with a particular edge of a support boundary is equal to the work done to rotate the vehicle body (which is subjected to gravitational as well as external and inertial forces/moments) about the edge, until the center of gravity reaches the equilibrium plane.

In computing the amount of the work, it should be noted that the gravity force is conservative while all other forces and moments are non-conservative. The energy stability level as defined above is a negative quantity for a stable condition. To be

consistent with the work of Messuri and Klein, we use the negative of this quantity, i.e., a positive value of energy stability level for a stable situation.

The main application of the extended measure of stability is for vehicles carrying a manipulator-like arm with considerable inertia such as those used in forestry and mining industries. Implementing this extended measure of stability would be easier if all destabilizing forces and moments other than weight are transferred to a common base. For vehicles carrying a manipulator-like tool, the manipulator base seems to be the best choice for this purpose.

3.1.2 Formulation

The calculation of energy stability level according to the definitions outlined in the previous section consists of three steps; finding the equilibrium plane, calculation of the work done to rotate the centre of gravity to the equilibrium plane (in the presence of only gravity loading), and finally calculation of the work done by all other destabilizing forces and moments other than gravity loading during the same rotation of the machine. Work calculations can also be classified as calculation of work done by conservative and non-conservative forces and moments. The gravity force is conservative which means the work done by it depends only on initial and final positions. The work done by other destabilizing forces and moments which are non-conservative, depends on the path travelled. The path chosen here is a circular curve which is formed when the machine is rotated around an edge of the support boundary.

Coordinate systems. Figure 3.4 shows the general coordinate systems used in the formulations. Frame **XYZ** is called 'machine coordinate frame' and is attached to the vehicle body at point P. This frame moves with the body. The selection of point P is arbitrary. For machines subject to this study which carry a manipulator

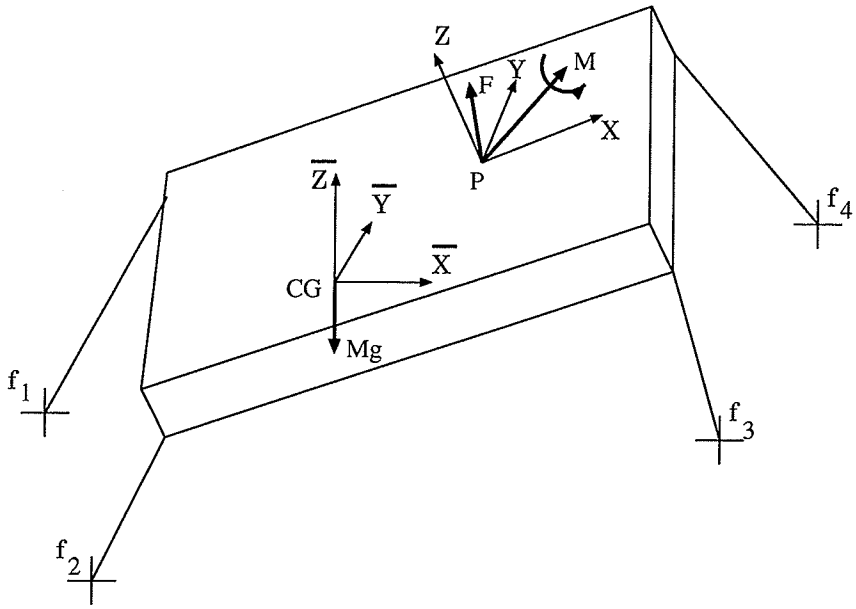

Figure 3.4: Machine and gravity coordinate frames.

arm the manipulator base is the most convenient selection (see also Figure 1.1). We assume that all forces and moments arising from the manipulation of the implement are known in this frame. Coordinates of contact points are also known in the machine frame.

Gravity frame $\bar{\mathbf{X}}\bar{\mathbf{Y}}\bar{\mathbf{Z}}$ is defined with the origin always at the centre of gravity of the machine. $\bar{\mathbf{Z}}$ is in direction opposite to acceleration of gravity, $\bar{\mathbf{X}}$ and $\mathbf{X}$ are in parallel planes; so are $\bar{\mathbf{Y}}$ and $\mathbf{Y}$ of $\mathbf{XYZ}$ frame. As the centre of gravity moves with respect to frame $\mathbf{XYZ}$, so does the base of the gravity frame. When machine is in a horizontal position machine frame $\mathbf{XYZ}$ is parallel to the gravity frame $\bar{\mathbf{X}}\bar{\mathbf{Y}}\bar{\mathbf{Z}}$.

In general, these two coordinate systems are separated by three translations, x_{CG}, y_{CG} and z_{CG} which are coordinates of the centre of gravity with respect to the machine frame $\mathbf{XYZ}$, and two attitudinal rotation angles for roll ϕ_x and pitch ϕ_y, both with respect to the machine frame (see Figure 3.5). Knowing the location of contact points f_1 and f_2 in the machine frame $\mathbf{XYZ}$, their location with respect to

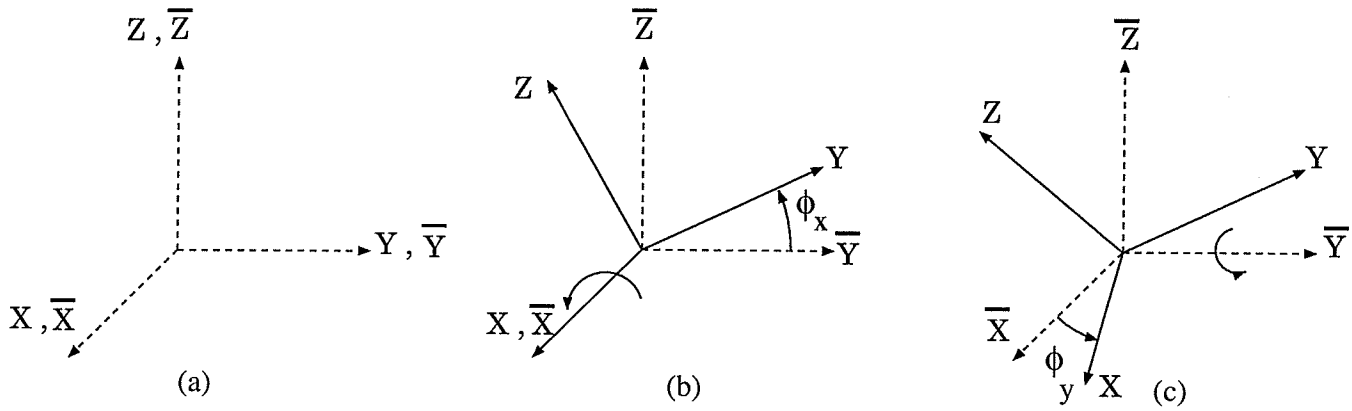

Figure 3.5: Roll and pitch rotations.

the gravity coordinate system $\bar{\mathbf{X}}\bar{\mathbf{Y}}\bar{\mathbf{Z}}$ are obtained from the following relation

$$\{f_1^*\} = \begin{bmatrix} f_{1x} \\ f_{1y} \\ f_{1z} \\ 1 \end{bmatrix}_{\bar{X}\bar{Y}\bar{Z}} = Rot(y,\phi_y)Rot(x,\phi_x)Trans(-x_{CG},-y_{CG},-z_{CG})\{f_1\} \quad (3.4)$$

$$\{f_2^*\} = \begin{bmatrix} f_{2x} \\ f_{2y} \\ f_{2z} \\ 1 \end{bmatrix}_{\bar{X}\bar{Y}\bar{Z}} = Rot(y,\phi_y)Rot(x,\phi_x)Trans(-x_{CG},-y_{CG},-z_{CG})\{f_2\} \quad (3.5)$$

$Rot(y,\phi_y), Rot(x,\phi_x)$ and $Trans(-x_{CG},-y_{CG},-z_{CG})$ are homogeneous transformation matrices defined as [13],

$$Rot(y,\phi_y) = \begin{bmatrix} cos\phi_y & 0 & sin\phi_y & 0 \\ 0 & 1 & 0 & 0 \\ -sin\phi_y & 0 & cos\phi_y & 0 \\ 0 & 0 & 0 & 1 \end{bmatrix} \quad (3.6)$$

$$Rot(x, \phi_x) = \begin{bmatrix} 1 & 0 & 0 & 0 \\ 0 & cos\phi_x & -sin\phi_x & 0 \\ 0 & sin\phi_x & cos\phi_x & 0 \\ 0 & 0 & 0 & 1 \end{bmatrix} \tag{3.7}$$

$$Trans(-x_{CG}, -y_{CG}, -z_{CG}) = \begin{bmatrix} 1 & 0 & 0 & -x_{CG} \\ 0 & 1 & 0 & -y_{CG} \\ 0 & 0 & 1 & -z_{CG} \\ 0 & 0 & 0 & 1 \end{bmatrix} \tag{3.8}$$

Vector description. The vector description of the system is described with reference to Figure 3.6. Here **XYZ** is the machine coordinates and point P is where all the forces and moments other than the weight are transferred to. $\bar{\mathbf{X}}\bar{\mathbf{Y}}\bar{\mathbf{Z}}$ is the gravity frame and CG is the location of the centre of gravity of the whole machine including the load at a given instant. f_1 and f_2 are the two adjacent contact points forming one edge of the support boundary. $\tilde{b}$ is the unit vector in direction of line connecting f_1 and f_2 and is described in **XYZ** coordinates as,

$$\tilde{b} = \frac{(\vec{f_2} - \vec{f_1})}{|\vec{f_2} - \vec{f_1}|} \tag{3.9}$$

where $\vec{f_1}$ and $\vec{f_2}$ are the position vectors of points f_1 and f_2 described in **XYZ** frame. $\vec{R}$ is a vector defined in **XYZ** frame, and is orthogonal to $f_1 f_2$. Note that,

$$\vec{R} \cdot \tilde{b} = 0 \tag{3.10}$$

We then define the vector $\vec{Cf_1}$ connecting point C to point f_1. $\vec{Cf_1}$ can be defined as,

$$\vec{Cf_1} = \lambda \tilde{b} \tag{3.11}$$

where λ is a constant depicting length of the vector $\vec{Cf_1}$. Knowing that,

$$\vec{f_1} + \lambda \tilde{b} = -\vec{R} \tag{3.12}$$

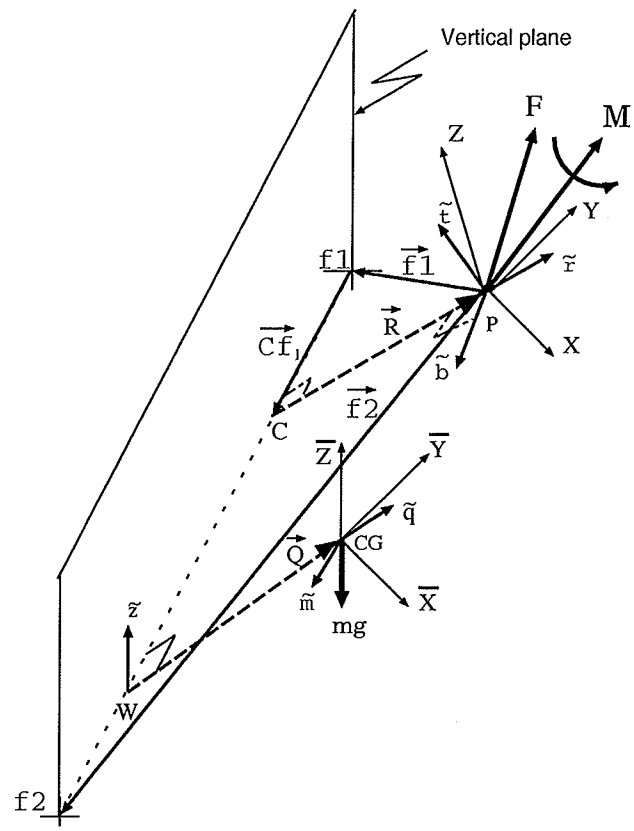

Figure 3.6: Vector description of the system.

then,

$$(\lambda\tilde{b} + \vec{f_1}) \cdot \tilde{b} = \vec{R} \cdot \tilde{b} = 0 \tag{3.13}$$

and

$$\lambda = \frac{(-\vec{f_1}) \cdot \tilde{b}}{b^2} \tag{3.14}$$

where b^2 =1. Therefore $\vec{R}$ could be found from,

$$\vec{R} = (\vec{f_1} \cdot \tilde{b})\tilde{b} - \vec{f_1} \tag{3.15}$$

Unit vector $\tilde{t}$ which is perpendicular to plane PCf_1 is now computed,

$$\tilde{t} = \tilde{b} \times \tilde{r} \tag{3.16}$$

where $\tilde{r} = \frac{\vec{R}}{|\vec{R}|}$ is the unit vector in the direction of $\vec{R}$.

Similarly vector $\vec{Q}$ is computed in the gravity coordinates $\bar{\mathbf{X}}\bar{\mathbf{Y}}\bar{\mathbf{Z}}$. Note that $\vec{Q}$ is orthogonal to line $f_1 f_2$ and is connected to the centre of gravity of the machine CG. $\vec{f_1^*}$ and $\vec{f_2^*}$ are the position vectors of points f_1 and f_2 in $\bar{\mathbf{X}}\bar{\mathbf{Y}}\bar{\mathbf{Z}}$ frame. $\tilde{m}$ is the unit vector in the direction of line connecting f_1 to f_2 in $\bar{\mathbf{X}}\bar{\mathbf{Y}}\bar{\mathbf{Z}}$ coordinate system and is given by,

$$\tilde{m} = \frac{(\vec{f_2^*} - \vec{f_1^*})}{|\vec{f_2^*} - \vec{f_1^*}|} \tag{3.17}$$

Again we have the following condition:

$$\vec{Q} \cdot \tilde{m} = 0 \tag{3.18}$$

Therefore $\vec{Q}$ could be found from,

$$\vec{Q} = (\vec{f_1^*} \cdot \tilde{m})\tilde{m} - \vec{f_1^*} \tag{3.19}$$

$\tilde{z}$ in Figure 3.6 is a unit vector in the direction of $\bar{\mathbf{Z}}$ and represents upward vertical direction.

Equilibrium plane. Equilibrium plane as described in *definition 9*, is a plane containing the support boundary edge $f_1 f_2$ and the centre of gravity with an orientation so that the summation of all moments around the boundary edge is minimum. Figure 3.7 shows the equilibrium plane for a general three dimensional case. The plane is described with an inclination angle of ϕ from the vertical plane. In this plane the following relation holds,

$$\sum_{around f_1 f_2} \mathcal{M} = (\vec{\mathbf{F}} \cdot \tilde{t})|\vec{R}| + \vec{\mathbf{M}} \cdot \tilde{b} + mg|\vec{Q}|cos\alpha \ \ sin\phi = 0 \tag{3.20}$$

note that a destabilizing moment has been assigned a positive sign. From Equation (3.20), angle ϕ is found as

$$\phi = -sin^{-1}\frac{(\vec{\mathbf{F}} \cdot \tilde{t})|\vec{R}| + \vec{\mathbf{M}} \cdot \tilde{b}}{mg|\vec{Q}|cos\alpha} \tag{3.21}$$

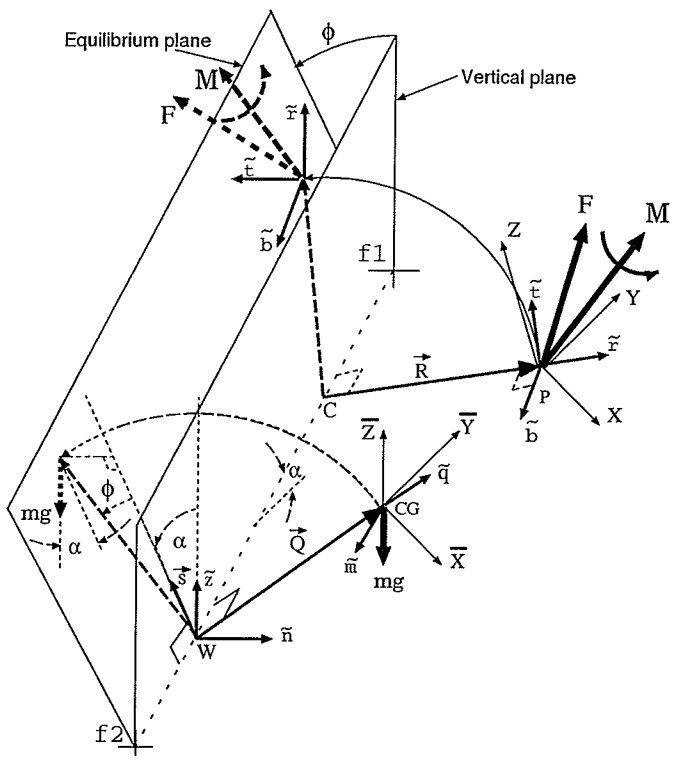

Figure 3.7: Finding the equilibrium plane.

Note that in Equation (3.21) vectors in the numerator are defined in **XYZ** frame and $\vec{Q}$ in denominator is defined in $\bar{\mathbf{X}}\bar{\mathbf{Y}}\bar{\mathbf{Z}}$ frame.

The only unknown in the right hand side of Equation (3.21) is the angle α representing the angle that support boundary edge, $f_1 f_2$, makes with a horizontal plane. To find α, we first find $\tilde{n}$ which is the normal to a plane constructed by $\tilde{z}$ and $\tilde{m}$ in $\bar{\mathbf{X}}\bar{\mathbf{Y}}\bar{\mathbf{Z}}$ frame (see Figure 3.7),

$$\tilde{n} = \frac{\tilde{z} \times \tilde{m}}{|\tilde{z} \times \tilde{m}|} \tag{3.22}$$

Another outer product between $\tilde{m}$ and $\tilde{n}$ yields the vector $\vec{s}$ which is in the vertical plane and perpendicular to the line $f_1 f_2$.

$$\vec{s} = \tilde{m} \times \tilde{n} \tag{3.23}$$

The angle α, can then be found from

$$\alpha = cos^{-1}(\tilde{z} \cdot \frac{\vec{s}}{|\vec{s}|}) \tag{3.24}$$

Note that when $\vec{\mathbf{F}}$ and $\vec{\mathbf{M}}$ are both zero, we would have $\phi = 0$ meaning the vertical plane is the equilibrium plane. Also note that Equation (3.21) has a solution only if

$$(\vec{\mathbf{F}} \cdot \tilde{t})|\vec{R}| + \vec{\mathbf{M}} \cdot \tilde{b} \leq mg|\vec{Q}|cos\alpha \tag{3.25}$$

When the above condition does not hold and the summation of moments around the support boundary edge is negative (special case), based on *definition 9* the angle ϕ is set to 90° (see Section 3.1.1). Therefore,

$$\phi = \begin{cases} -sin^{-1}\frac{(\vec{\mathbf{F}}\cdot\tilde{t})|\vec{R}|+\vec{\mathbf{M}}\cdot\tilde{b}}{mg|\vec{Q}|cos\alpha} & when \quad (\vec{\mathbf{F}} \cdot \tilde{t})|\vec{R}| + \vec{\mathbf{M}} \cdot \tilde{b} \leq mg|\vec{Q}|cos\alpha \\ 90° & when \quad (\vec{\mathbf{F}} \cdot \tilde{t})|\vec{R}| + \vec{\mathbf{M}} \cdot \tilde{b} > mg|\vec{Q}|cos\alpha \end{cases} \tag{3.26}$$

Work calculation for conservative forces. Figure 3.8 shows the method of calculating the first part of energy stability level from *definition 10*, which is the work done when the centre of gravity is rotated around a support boundary edge to the equilibrium plane. As the weight force is conservative, the work done depends only on the vertical displacement of centre of gravity h

$$W_1 = -mgh$$

where h is computed from the following relation,

$$h = |\vec{Q}|(cos\phi - cos\psi)cos\alpha \tag{3.27}$$

the angle ψ between $\vec{Q}$ and the vertical plane is

$$\psi = cos^{-1}(\tilde{q} \cdot \frac{\tilde{s}}{|\tilde{s}|}) \tag{3.28}$$

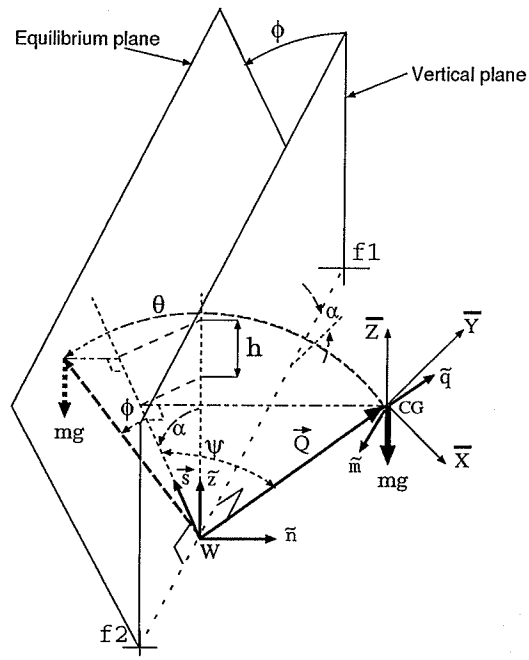

Figure 3.8: Work done by gravitational force.

where $\tilde{q}$ is a unit vector in direction of $\vec{Q}$. Note that all these vectors are defined in the $\bar{\mathbf{X}}\bar{\mathbf{Y}}\bar{\mathbf{Z}}$ frame. Therefore the part of the energy stability level associated with conservative forces based on *definition 10* is computed from,

$$W_1 = -mg|\vec{Q}|[cos\phi - cos\psi]cos\alpha \tag{3.29}$$

Note that total hypothetical rotation of the machine is

$$\theta = \phi + \psi \tag{3.30}$$

Work calculation for non-conservative forces and moments. The second part of energy stability level calculation consists of calculating the work done by destabilizing forces and moments other than the weight forces. This is the work done during the hypothetical rotation of the machine over a support boundary edge until the onset of instability occurs. Figure 3.9 shows the same edge of support boundary

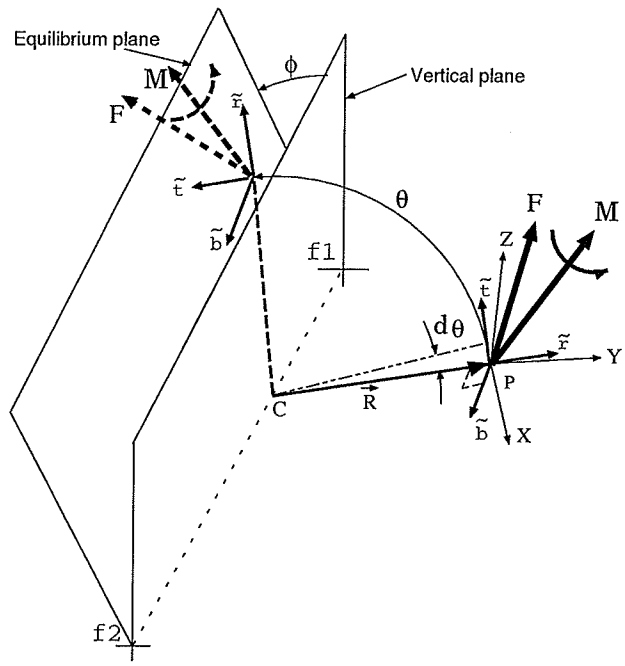

Figure 3.9: Work done by non-conservative forces and moments.

shown in Figure 3.8. The work done by the resultant forces and moments can be calculated from,

$$W_2 = \int (\vec{\mathbf{F}} \cdot \tilde{t}) ds + \int (\vec{\mathbf{M}} \cdot \tilde{b}) d\theta \tag{3.31}$$

where

$$ds = |\vec{R}| d\theta$$

Therefore,

$$W_2 = \int (\vec{\mathbf{F}} \cdot \tilde{t}) |\vec{R}| d\theta + \int (\vec{\mathbf{M}} \cdot \tilde{b}) d\theta \tag{3.32}$$

vectors are defined in the **XYZ** frame. During the hypothetical rotation of the machine over the edge of the support boundary, $f_1 f_2$, the direction of external forces and moments do not change relative to the machine frame **XYZ**. The reason is that the direction of these forces and moments does not depend on the orientation of the machine frame with respect to the gravity frame. Therefore the two inner products

under integral sign remain constant, i.e.,

$$\vec{\mathbf{F}} \cdot \tilde{t} = const. \tag{3.33}$$

$$\vec{\mathbf{M}} \cdot \tilde{b} = const. \tag{3.34}$$

and we have,

$$\begin{aligned} W_2 &= (\vec{\mathbf{F}} \cdot \tilde{t})|\vec{R}| \int d\theta + (\vec{\mathbf{M}} \cdot \tilde{b}) \int d\theta \\ &= [(\vec{\mathbf{F}} \cdot \tilde{t})|\vec{R}| + (\vec{\mathbf{M}} \cdot \tilde{b})]\theta \end{aligned} \tag{3.35}$$

where θ is determined from Equation (3.30),

Total energy stability level. According to definition 10, energy stability level for each edge of the support boundary such as $f_1 f_2$ is,

$$Energy\ Stability\ Level_{f_1 f_2} = -(W_1 + W_2) \tag{3.36}$$

Therefore at each instant, the energy stability level will be calculated for every edge of the support boundary. Margin of energy stability is then the minimum of all energy stability levels obtained for each edge of the support boundary.

3.2 Application to Mobile Heavy-Duty Machines

The extended measure of stability has been developed in Section 3.1. In this section implementation aspects of the algorithm for stability analysis of mobile heavy-duty hydraulic manipulators are discussed. From Section 3.1, we know that the energy stability level for each edge of the support boundary is a function of the following variables

$$Energy\ Stability\ Level = \mathcal{F}(f_1, f_2, \phi_x, \phi_y, m_{total}, \vec{R}_{CG}, \vec{\mathbf{F}}, \vec{\mathbf{M}}) \tag{3.37}$$

f_1 and f_2 are the coordinates of feet contact points which form the adjacent points in the support boundary. These coordinates are measured with respect to the machine frame **XYZ**. ϕ_x and ϕ_y are the measured machine base deviations, from the level position (roll and pitch angles). m_{total} represents the total mass of the machine including the load. The location of the combined centre of gravity represented by position vector $\vec{R}_{CG}$ is another input variable to Equation (3.37). This position vector is again computed with respect to the machine frame **XYZ**. Finally, $\vec{\mathbf{F}}$ and $\vec{\mathbf{M}}$ represent external forces and moments, originated from interaction with environment and/or movements of the arm of the machine manipulator.

Figure 3.10 shows the flow chart of a stability analysis algorithm for a mobile heavy-duty hydraulic manipulator. The operator's control commands (voltages) to the hydraulic valves together with the physical parameters of the machine and external loads determine the manipulator's joint positions, velocities and accelerations. In our study these quantities are produced by the simulation program.

Displacements of the manipulator arm change the location of the centre of gravity according to the relation:

$$\vec{R}_{CG} = \begin{bmatrix} x_{CG} \\ y_{CG} \\ z_{CG} \end{bmatrix} = \frac{\sum_{i=1}^{n} m_i {}^0\hat{\vec{s}}_i + M_{load} {}^0\hat{\vec{s}}_{load} + M_{vehicle} \hat{\vec{r}}_{vehicle}}{\sum_{i=1}^{n} m_i + M_{load} + M_{vehicle}} \tag{3.38}$$

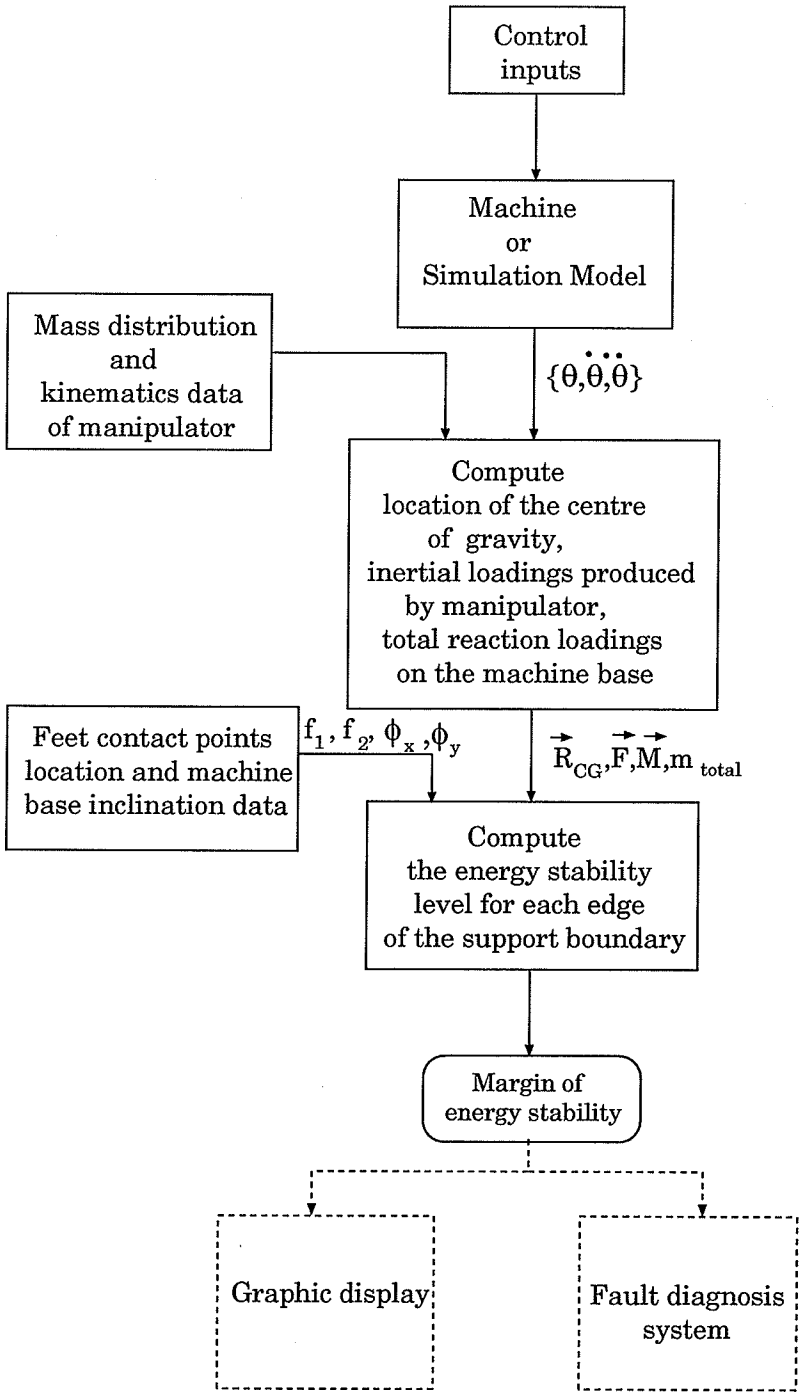

Figure 3.10: Flow chart for stability analysis.

where $\vec{R}_{CG}$ is the position vector of the centre of gravity and ${}^0\hat{\vec{s}}_i$ is the position vector of the ith link of the manipulator, both expressed in the machine frame **XYZ**. The location of the centre of gravity of each link is usually known with respect to the frame attached to the link. To compute ${}^0\hat{\vec{s}}_i$ kinematics of the manipulator must be known. Kinematics of the manipulator is defined by the link frame attachments and link parameters [15]. Once the link frames have been defined, the link transformation matrices,${}^0A_1, {}^1A_2, ..., {}^{i-1}A_i$, which define the kinematics of the manipulator can be computed from Denavit-Hartenberg (D-H) transformation technique for adjacent coordinate frames [15]. D-H transformation matrices are then used to compute ${}^0\hat{\vec{s}}_i$ from the following relation:

$$\begin{bmatrix} {}^0\hat{\vec{s}}_i \\ 1 \end{bmatrix} = {}^0A_1{}^1A_2...{}^{i-1}A_i{}^is_i = {}^0A_i \begin{bmatrix} \bar{x}_i \\ \bar{y}_i \\ \bar{z}_i \\ 1 \end{bmatrix} \tag{3.39}$$

where $(\bar{x}_i, \bar{y}_i, \bar{z}_i)$ are the coordinates of the center of gravity of ith link in its own frame. $M_{vehicle}$ and ${}^0\hat{\vec{r}}_{vehicle}$, in Equation (3.38), are the weight and the position vector of the centre of gravity of the machine base, respectively. ${}^0\hat{\vec{s}}_{load}$ is the position vector of the centre of gravity of the load in **XYZ** frame and is obtained from the following transformation:

$${}^0\hat{\vec{s}}_{load} = {}^0A_n{}^nA_{load}\ {}^{load}\hat{\vec{s}}_{load} \tag{3.40}$$

where ${}^nA_{load}$ is the homogeneous transformation between the load and the manipulator's last link frame.

In the next step, external force and moment vectors ($\vec{\mathbf{F}}$ and $\vec{\mathbf{M}}$) exerted on the machine base must be computed. This includes the computation of the reaction forces and moments produced at the manipulator base while carrying a load or interacting with the environment excluding the gravitational components. This is in fact an

inverse dynamic problem. Newton-Euler dynamic formulation [16] is adopted for this purpose. This formulation represents an efficient set of equations of motion for a manipulator. The method consists of an outward and an inward iteration loop (see Figure 3.11).

In the outward iteration, first the rotational and linear velocity and acceleration of each link is computed by propagating velocities and accelerations from the first link to the last one. Angular velocity of manipulator links are calculated from:

$$^{i+1}\vec{\omega}_{i+1} = {}^{i+1}R_i({}^{i}\vec{\omega}_i + \vec{z}_0\dot{\theta}_{i+1}) \tag{3.41}$$

where ${}^{i}R_{i+1} = ({}^{i+1}R_i)^T$ is the rotation part of the Denavite-Hartenberg transformation matrix for each link, $\dot{\theta}$ is the joint angular velocity known from the trajectory and $\vec{z}_0$ is defined as:

$$\vec{z}_0 = \begin{bmatrix} 0 \\ 0 \\ 1 \end{bmatrix} \tag{3.42}$$

Angular acceleration of the manipulator links are computed from:

$$^{i+1}\dot{\vec{\omega}}_{i+1} = {}^{i+1}R_i[{}^{i}\dot{\vec{\omega}}_i + \vec{z}_0\ddot{\theta}_{i+1} + {}^{i}\vec{\omega}_i \times (\vec{z}_0\dot{\theta}_{i+1})] \tag{3.43}$$

where $\ddot{\theta}$ is the angular acceleration of the manipulator joint. Velocity and acceleration of each link are calculated from:

$$^{i+1}\vec{v}_{i+1} = ({}^{i+1}\vec{\omega}_{i+1}) \times ({}^{0}R_{i+1}\vec{P}^*_{i+1}) + {}^{i+1}R_i{}^{i}\vec{v}_i \tag{3.44}$$

$$^{i+1}\dot{\vec{v}}_{i+1} = {}^{i+1}\dot{\vec{\omega}}_{i+1} \times ({}^{0}R_{i+1}\vec{P}^*_{i+1}) + {}^{i+1}\vec{\omega}_{i+1} \times [{}^{i+1}\vec{\omega}_{i+1} \times ({}^{0}R_{i+1}\vec{P}^*_{i+1})] + {}^{i+1}R_i{}^{i}\dot{\vec{v}}_i \tag{3.45}$$

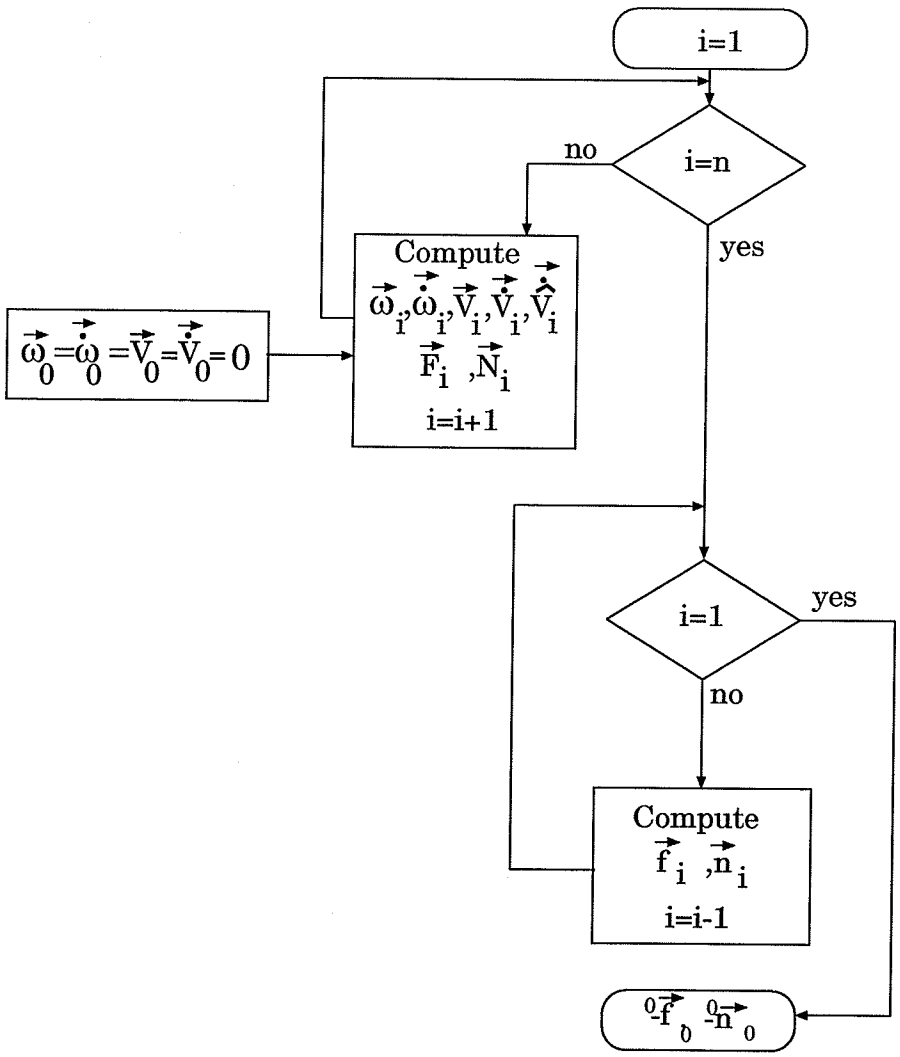

Figure 3.11: Calculation of reaction force and moment exerted by the manipulator.

and acceleration of the centre of the gravity ${}^i\dot{\hat{\vec{v}}}_i$ is obtained from:

$$ {}^i\dot{\hat{\vec{v}}}_i = {}^i\dot{\vec{\omega}}_i \times {}^i\hat{\vec{s}}_i + {}^i\vec{\omega}_i \times ({}^i\vec{\omega}_i \times {}^i\hat{\vec{s}}_i) + {}^i\dot{\vec{v}}_i \tag{3.46} $$

where ${}^0R_i\vec{P}_i^*$ is defined as:

$$ {}^0R_i\vec{P}_i^* = \begin{bmatrix} a_i \\ d_i sin\alpha_i \\ d_i cos\alpha_i \end{bmatrix} \tag{3.47} $$

where d_i and α_i are kinematic parameters of link i (see Appendix B). Note that $\vec{\omega}_0 = \dot{\vec{\omega}}_0 = \vec{v}_0 = 0$. We will also assign $\dot{\vec{v}}_0 = 0$ since we are only interested in calculating the reaction forces and moments excluding the gravitational effect. Inertial forces and torques acting at the centre of mass of each link is calculated from the relation

$$ {}^i\vec{F}_i = m_i {}^i\dot{\hat{\vec{v}}}_i \tag{3.48} $$

$$ {}^i\vec{N}_i = {}^iI_i {}^iR_0 {}^i\dot{\vec{\omega}}_i + {}^i\vec{\omega}_i \times [({}^iI_i {}^iR_0) {}^i\vec{\omega}_i] \tag{3.49} $$

where ${}^iI_i$ are the elements of the inertia tensor matrix (see Appendix B). The reaction forces and torques acting at each joint is computed in the inward loop of Figure 3.12. It begins from the last link and is computed from the following relations:

$$ {}^i\vec{\mathbf{f}}_i = {}^{i+1}R_i {}^{i+1}\vec{\mathbf{f}}_{i+1} + {}^i\vec{F}_i \tag{3.50} $$

$$ {}^i\vec{\mathbf{n}}_i = {}^{i+1}R_i[{}^{i+1}\vec{\mathbf{n}}_{i+1} + ({}^0R_{i+1}\vec{P}_i^*) \times {}^{i+1}\vec{\mathbf{f}}_{i+1}] + ({}^0R_i\vec{P}_{i+1}^* + {}^i\hat{\vec{s}}_i) \times {}^i\vec{F}_i + {}^i\vec{N}_i \tag{3.51} $$

Note that

$$ {}^{n+1}\vec{\mathbf{n}}_{n+1} = {}^{load}n_{load}, \quad {}^{n+1}\vec{\mathbf{f}}_{n+1} = {}^{load}f_{load} \tag{3.52} $$

n is the number of links and ${}^{load}n_{load}$ and ${}^{load}f_{load}$ are respectively external moments and forces due to contact with the environment and are expressed in the load frame. Finally the resultant vectors of forces and moments exerted by the manipulator on the machine base are

$$ \vec{\mathbf{F}} = -{}^0\vec{\mathbf{f}}_0 \tag{3.53} $$

$$\vec{\mathbf{M}} = -{}^{0}\vec{\mathbf{n}}_0 \tag{3.54}$$

The next step in the algorithm is the energy stability level calculations using the formulation in Section 3.1.

Chapter 4

Stability Study of An Excavator Based Machine

4.1 Description of the Machine

In this chapter the algorithm developed in Chapter 3 is used to study the stability of a typical mobile heavy-duty hydraulic manipulator. The machine, a 215B Caterpillar excavator based machine, is shown in Figure 4.1. It is a mobile three-degree-of-freedom manipulator with an end-effector. The end-effector can be a bucket or it can be a gripper for holding and handling objects such as trees. The upper structure of the excavator is turned on the carriage by a swing motor through a gear train. Boom and stick are the other two links which, together with the swing, serve to position the end-effector. Each link is activated by means of flow and pressure through the main valves. Modulation of the oil flow in the main valves is controlled by a pilot system through joysticks 1 and 2 (see Figure 4.1); forward, backward or side to side movements of these levers provide individual control of the link motion.

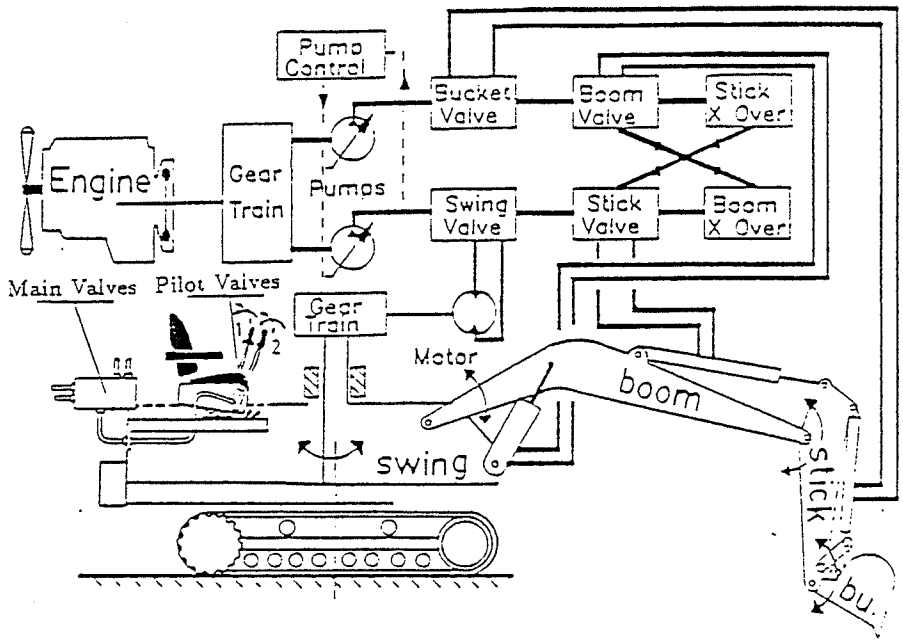

Figure 4.1: 215B Caterpillar excavator based log loader.

Figure 4.1 also shows the main actuation circuit. The output of the engine is used to turn two pumps. The output flow of the pumps is used to operate the hydraulic cylinders and the swing motor. Hydraulic oil from pump 1 passes through swing, stick and boom cross-over valves to the tank. Stick movement controlled by the stick main valve, cannot be achieved if the swing main valve is fully open. If the latter is partly open, the stick can operate but at a slower speed. The motion of the boom and the stick are coupled via cross-over valves. This will allow a faster movement of one when the other is at less than full speed operation. When the total sum of the pressures in the implement circuit becomes high enough, the pumps reduce their outputs to prevent engine stall. This type of hydraulic circuit is known as a torque-limited circuit. The machine dynamics is complex and nonlinear in both the structure and the actuation. Kinematics and dynamic specification of the machine, including link frame attachments and the D-H transformation matrices are described in Appendix B.

For stability studies of the machine, the manipulator joints trajectories, i.e., joint displacements, velocities and accelerations are required. This information is normally obtained by direct measurement from the manipulator. For this study however, instead of the actual measurements we used the simulation model of the manipulator developed previously [17]. The validity of the simulation program has been tested before and has been reported elsewhere [18]. The simulation program was further improved by adding two modifications. First, to investigate the effect of operation over a gradient on the stability of the machine, it was necessary to include the effect of a non-level base in the dynamic behavior of the manipulator arm. This was done by modifying the Lagrangian dynamic equation of the manipulator. Another necessary modification was to model the end-of-stroke condition in the manipulator's hydraulic actuators. Since hydraulic actuators are known to generate a significant dynamic shock force when reaching their limits [19], it was necessary to model this phenomenon to be able to evaluate its effect on the stability of the machine. A simple yet effective method was proposed and was verified by experiment. Details of the above modifications are included in Appendix C.

4.2 Simulation Studies

To explore the effect of different operating conditions on the stability of the machine a number of simulations are performed. It is also shown how simulation studies can be used to put necessary safety limits on loads, velocities and forces in different configurations so that the safety of the machine and operator is guaranteed. Presently these kind of limitations only concern the load and radius of the end-effector position (static stability) and velocity adjustments are left to the skill and experience of the operator [1]. It is shown in this chapter that dynamic effects are sometimes as important as the static effects and put limitations on the machine operating conditions.

Another application of such a simulation study is to provide the designers with an inexpensive, fast and safe tool to fine tune the design details of different parts of the machine based on the stability criteria. One example of these design details could be the weight and location of the counterweight in the cabin of the machine.

4.2.1 Effect of a sudden stop

Figure 4.2 shows the results of a typical machine operation involving swing motion. Note that **XY** in this figure represents the machine frame **XYZ** (see Section 3.1). Given a step voltage command, the machine rotated from initial position $\theta = 90°$ and was brought to stop after one full revolution at $\theta = 270°$. Figure 4.2a shows the swing valve's spool displacement response to the voltage command. The response is that of a first degree system with a time constant of τ. The changes in the input and output pressures of the swing hydraulic motor are shown in Figure 4.2b. The limiting pressure in the system due to existence of the relief valve was 27.6 (MPa.). Pressures beyond this limit cause the relief valve to open. From stability point of view the action of relief valve has both favorable and unfavorable effects which will be discussed later.

Displacement, velocity and acceleration profiles for swing joint are shown in Figure 4.2c. Accelerations and therefore inertial forces and moments are much higher during the start and the stop of the motion. Referring to Figure 4.2c, when the command voltage is set to zero (at $t \approx 10$ s), the acceleration goes to a minimum and stays flat for a duration of time. This saturation is the result of the relief valve action mentioned above. Note that after the command voltage has been set to zero ($\theta = 450°$), the swing joint continued to rotate up to $\theta = 459°$. This overriding is

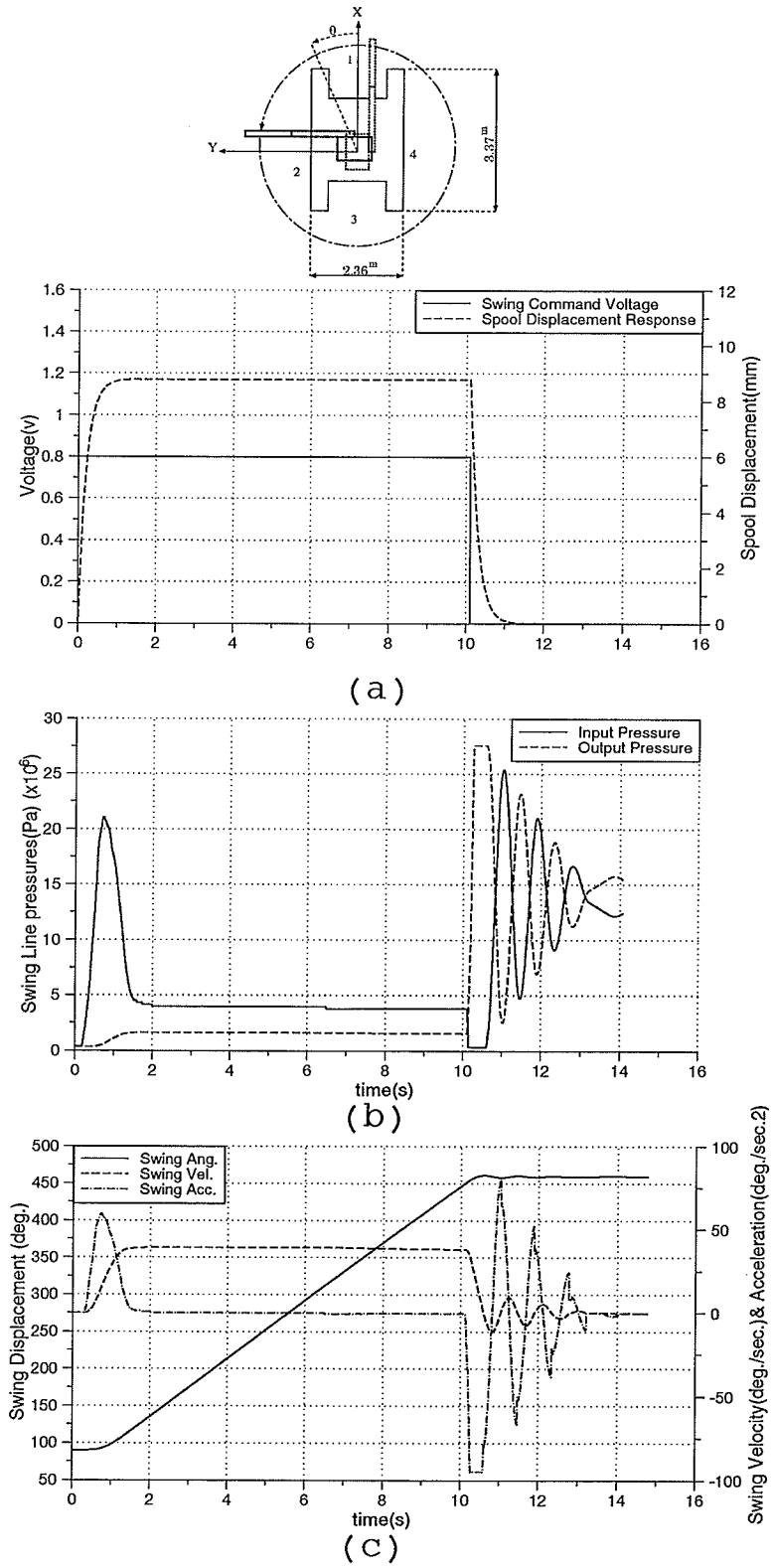

Figure 4.2: Typical swing motion.

again a result of the pressure saturation caused by the relief valve action.

Figure 4.3 depicts the reaction moments (Figure 4.3a) and forces (Figure 4.3b) developed at the manipulator base during the motion. These moments and forces are due to inertial, centrifugal and Coriolis forces produced at the manipulator joints. Note that the reaction moment and force about the Z axis of the machine has no effect on its stability.

Figure 4.4 shows the results of the stability analysis based on the machine response demonstrated in Figure 4.2. Changes in the energy stability level as the swing joint rotated is shown in Figure 4.4a. These are a result of changes in the centre of gravity position and the reaction forces and moments produced by the manipulator. Figure 4.4b compares the energy stability level for two edges of the support boundary (edges 1 and 3) using the extended measure of stability developed in this thesis, with the one obtained by the energy stability level concept as defined in [4] (i.e., without the effect of inertial forces and moments). The largest deviation is at the instant of stop when large inertial forces and moments were present. During the steady-state motion of the manipulator ($2 < t < 10s$), the inertial loadings were zero and the difference in energy stability level was caused by the centrifugal and Coriolis forces/moments (see Figure 4.3).

The software package used for this and other simulation studies in this chapter was developed by implementing the algorithm in Section 3.2 and was written in "C" language. The average running time on a *Spark 2 Sun* workstation for computation of energy stability levels for a four sided support boundary was approximately 0.0178 seconds. Calculation of the external and inertial forces and moments took approximately 0.0148 seconds of the total running time. Therefore the program can easily run at a 50 Hz. sampling rate.

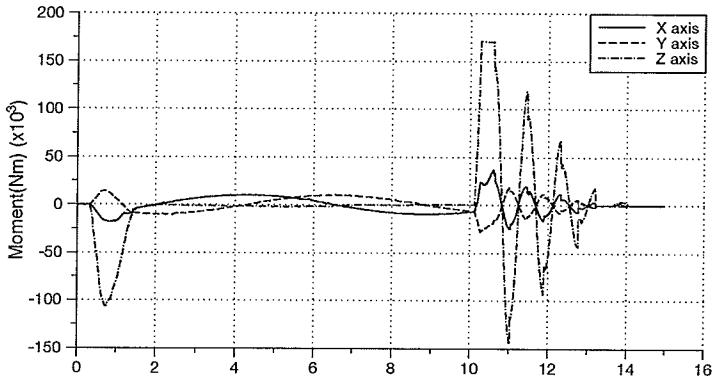

(a)

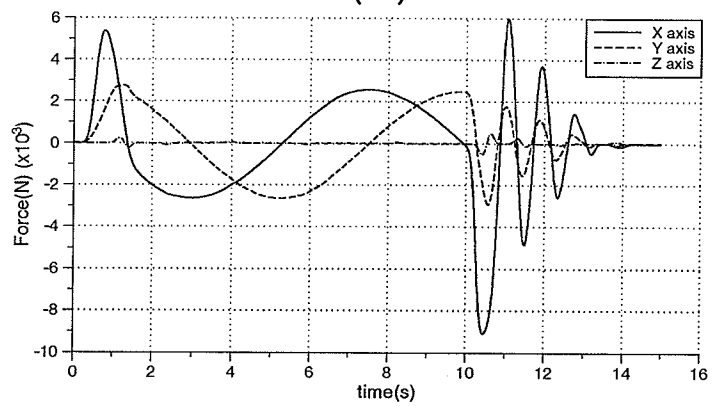

(b)

Figure 4.3: Reaction moments and forces at the manipulator base.

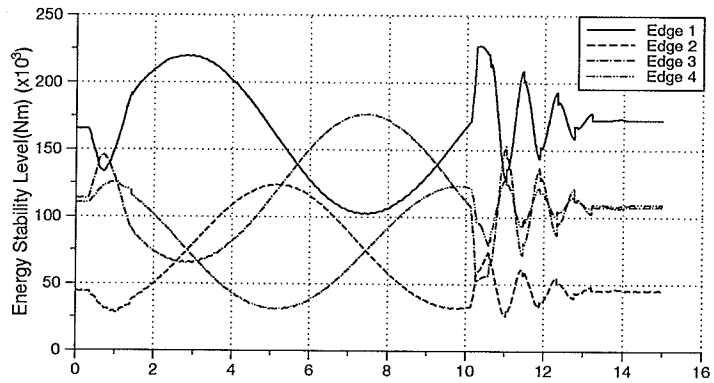

(a)

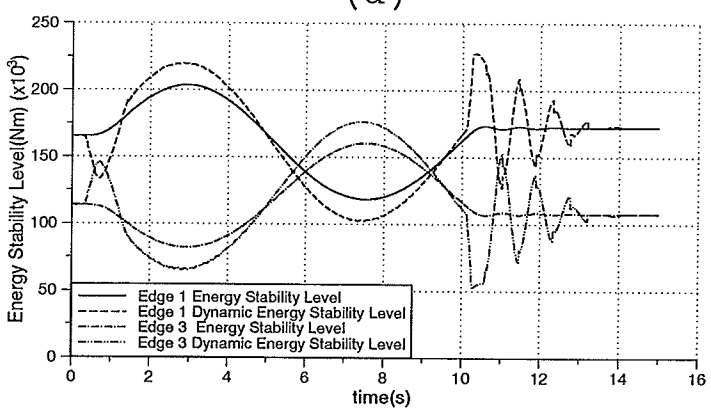

(b)

Figure 4.4: Typical stability analysis results.

4.2.2 Effect of swing velocity

From previous experiments it was observed that the main destabilizing occurs when the machine is brought to a sudden stop. In this case study we applied different command voltages which brought the cab to different swing velocities. Once the steady-state was achieved and the swing angle reached at 90° the command voltage was set to zero. This way the only variable was the swing velocity. The experiment was repeated with two different link configurations: *In* configuration (θ_{boom}=43 and θ_{stick}=-115), and *Out* configuration (θ_{boom}=0 and θ_{stick}=-80). The results shown in Figure 4.5a depicts the minimum margin of stability which has occurred for each swing velocity (in this experiment side 2 had the minimum energy stability level). Figure 4.5a also shows that, for velocities less than 20 deg./sec., the stability decreases with the increased velocity, and the '*out*' configuration shows a lower stability level compared to the '*in*' configuration. This was expected since the machine has a larger inertia while it is in the '*out*' configuration and therefore a larger destabilizing inertial loading exists. For rotational velocities higher than 20 deg./sec. the margin of stability is almost equal for both configurations and remains basically the same with increasing the velocity. This can be explained by considering the acceleration profile. Referring to Figure 4.5b, for velocities higher than 20 deg./sec., acceleration reaches a saturation limit at the time of stopping for both '*in*' and '*out*' configurations (Figure 4.5b compares the result for the swing velocity of 30 deg./sec.). This happens because of the relief valve action in limiting the pressures in the hydraulic line. When the command voltage is set to zero, the hydraulic motor tries to stop the manipulator and the outlet pressure builds up (similar to situation depicted in Figure 4.2b). The moment M that the hydraulic motor can exert to stop the manipulator is proportional to the pressure difference in hydraulic motor which is now limited by the relief valve. Since $M = I\alpha$, the maximum deceleration produced by the hydraulic system has a bound as shown in Figure 4.5b.

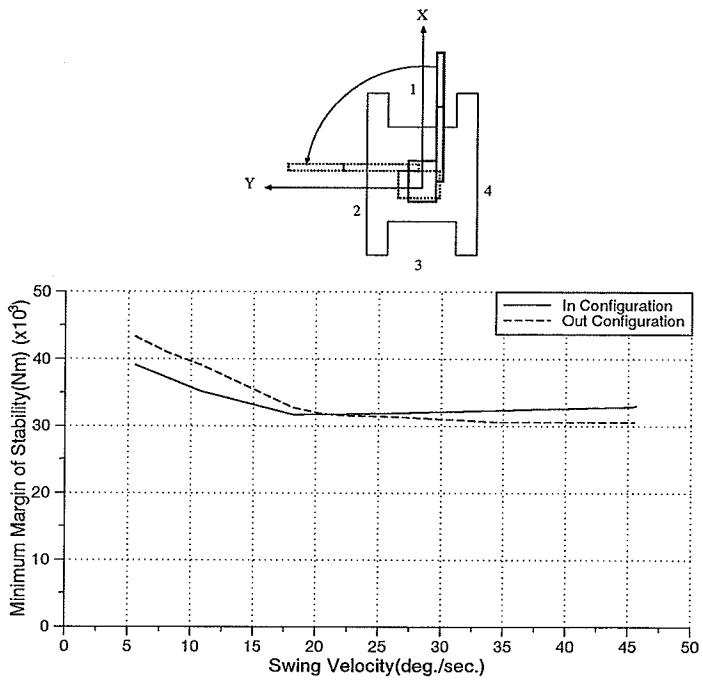

(a)

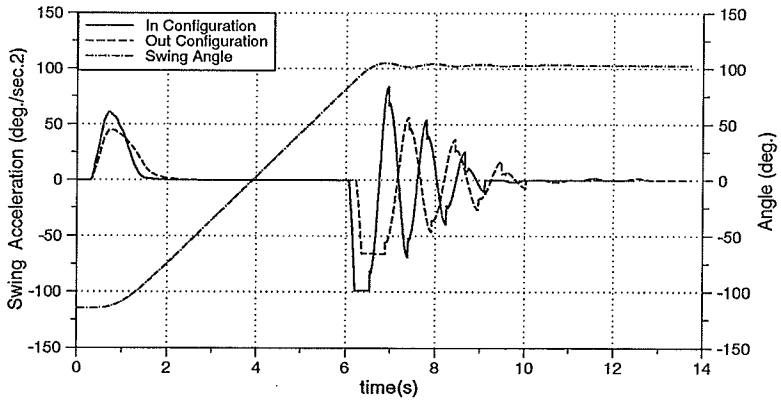

(b)

Figure 4.5: Effect of swing motion.

Note also that combined moment of inertia is larger for '*out*' configuration, i.e., ($I_{out} > I_{in}$), therefore we should have $\alpha_{out_{limit}} < \alpha_{in_{limit}}$ which is consistent with the result shown in Figure 4.5b. Therefore for swing velocities higher than 20 deg./sec., the relief valve smooths the stopping action and as a result keeps the inertial loadings within a limit. This can be considered favorable for the machine stability purposes but may result in overriding of the swing rotation (similar to situation depicted in Figure 4.2c) which could be undesirable since the manipulator arm cannot be stopped at a desired position. The slight increase in the stability margin for the '*out*' configuration case in Figure 4.5a is caused by the same overriding as a result of which the manipulator passes $\theta = 90°$ which is the position with minimum static stability.

4.2.3 Effect of the load mass

The effect of load mass on the stability of the machine is now investigated. Consistent with the setup in the Section 4.2.2, we kept the swing velocity constant ($\approx$ 30 deg./sec.) and increased the mass load carried by the manipulator. The swing was brought to stop at $\theta = 90°$. Figure 4.6a shows the margin of energy stability for three different loads (the minimum energy stability level was associated with side 2). Increasing the load decreased the static stability and at the same time reduced the effect of inertial loading on the stability of the machine. As a result the dynamic and static margins of energy stability approached the same value. Figure 4.6b shows this trend clearly. The dampening of the dynamic effects is again the result of the limit on the maximum pressure allowed in the hydraulic lines. As the load increased the maximum deceleration and therefore inertial loadings at time of stopping the machine decreased and so did the contribution of the inertial loads on the machine stability.

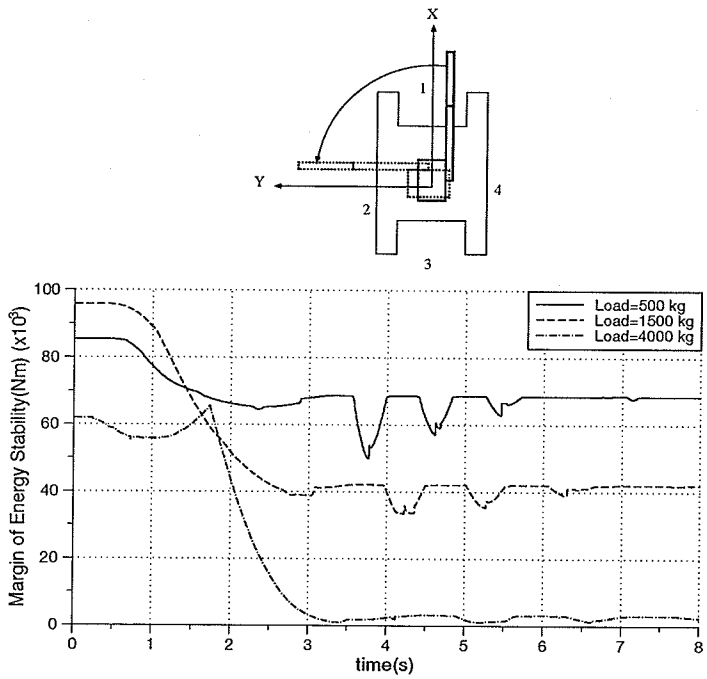

(a)

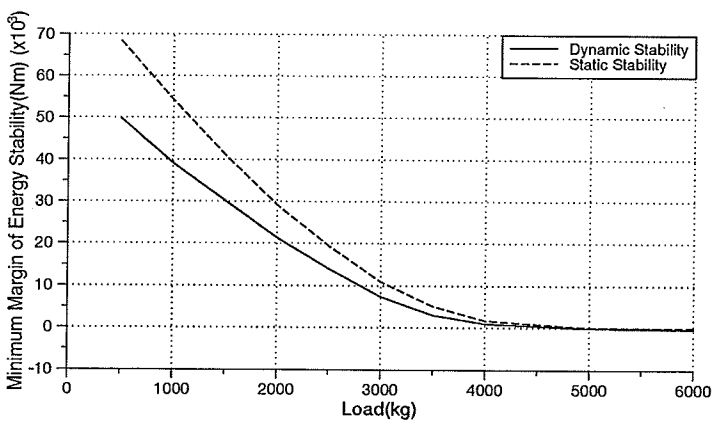

(b)

Figure 4.6: Effect of load mass.

4.2.4 Effect of the load inertia

Figure 4.7 shows the result of investigating the effect of the load inertia on the stability of the machine. In this set of experiments, weight (1500 kg), location of the centre of gravity and the swing velocity ($\approx$ 30 deg./sec.) were kept constant while the moment of inertia of the load was changed by varying the I_{xx} component of the inertia matrix of the load. This resembles the pick and place task for logs of similar mass but different length and thickness.

The difference between the two orientations of grabbing the log was also investigated. Results show that orientation 2 (see Figure 4.7) is insensitive to the changes in the load inertia in that the margin of stability remained the same with the increase of the load inertia. For orientation 1 however, the margin of stability decreased with the increase of the load inertia. Figure 4.7b shows the reaction moments produced at the manipulator base for I_{xx}=11800 ($kg.m^2$). It is seen that the inertial loading is higher in orientation 1 and that is the reason for the reduced stability. Components of overall inertia matrix which produce the moments about X and Y axes, are in general larger when the load is grabbed as in orientation 1.

4.2.5 Effect of top-heaviness

Effect of top-heaviness on the stability condition of the machine is shown in Figure 4.8. In this experiment a concentrated load is carried by the manipulator. In both configurations 1 and 2, load (1500 kg), velocity ($\approx$30 deg./sec.) and the position of the centre of gravity in horizontal plane are the same. Therefore the only difference between two configurations is the vertical position of the centre of gravity which represents the top-heaviness. The difference between the vertical position of the center of gravity for configurations 1 and 2 is 72.0 cm. The figure shows the margin

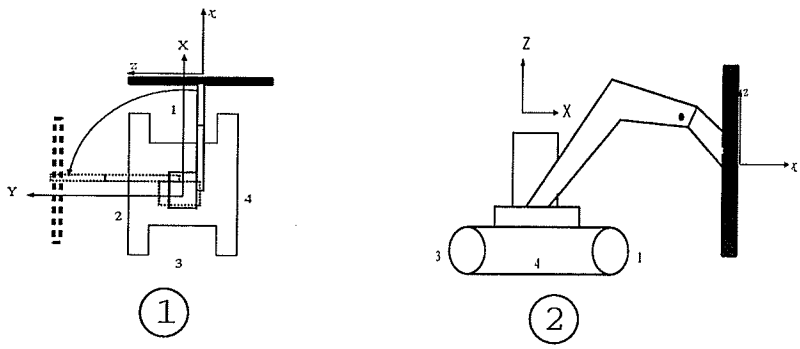

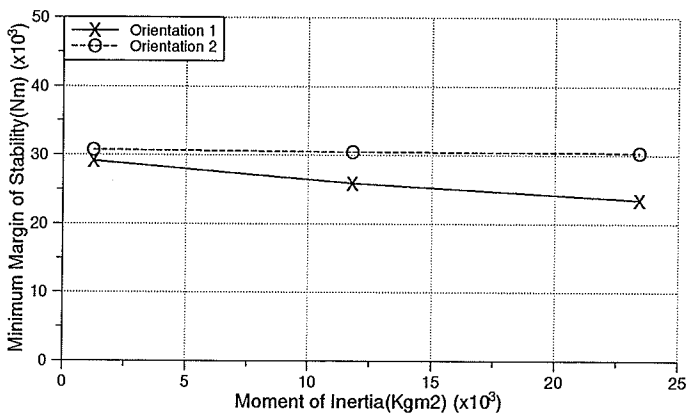

(a)

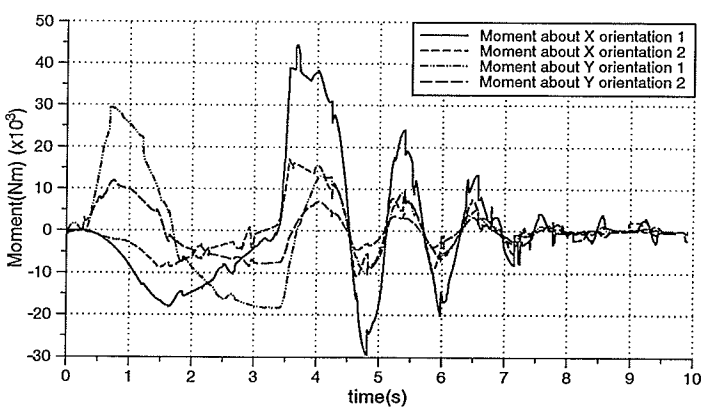

(b)

Figure 4.7: Effect of load inertia.

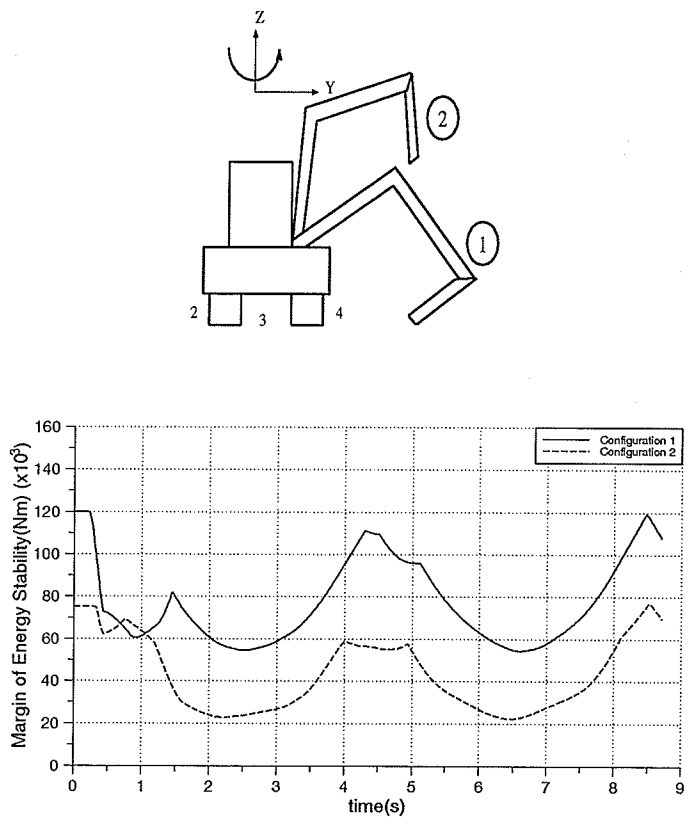

Figure 4.8: Effect of top-heaviness.

of energy stability when the swing joint has completed a full turn. The result shows that the margin of energy stability is reduced by increasing the top-heaviness. This reduction cannot be shown by either projection method or the method of Davidson and Shewitzer [6].

4.2.6 Effect of operation on a gradient

Machine stability when it is operating on a gradient is shown in Figure 4.9 (note that α in Figure 4.9 is equal to $-\phi_y$ as defined in Section 3.1). Here we simulated a full rotation of swing with the same conditions as in Figure 4.2, i.e., constant step

command voltage and load mass. The velocity was slightly different because of the gradient effect. Comparing Figure 4.4b with Figure 4.9a a slight decrease in the energy stability level for edges 2 and 4 is observed. The main difference occurs, however, for edges 1 and 3 where the energy stability level for edge 1 has been increased because it was on the uphill side, and the energy stability level of edge 3 has been dramatically decreased. Figure 4.4b shows the simulation of the same maneuver by the swing joint when the machine is positioned across the gradient. This caused the energy level of stability for edge 2 to reduce significantly. Referring to Figure 4.9b, at times $t \approx 1$ sec. and $t \approx 10$ sec., the energy stability levels for side 2 were almost zero meaning that the machine was on the verge of instability.

4.2.7 Effect of boom and stick motions

In this experiment we study the effect of boom and stick joint motions on the stability. Referring to Figure 4.10a, boom and stick started from the lowest position with average angular velocities of 9.0 and 16.0 deg./sec, respectively. The stick stopped due to reaching the end of its travel limit ($\approx$-30 deg.) and the boom was brought to a stop by setting the command voltage to zero when it reached at 50° (travel limit for boom joint is 58°). Figure 4.10b shows the energy stability levels during the motion. The rise in the vertical position of the centre of gravity increased the top heaviness and thus reduced the stability for all edges of the support boundary. When the stick reached its joint limit by the physical limitation of the mechanism, a noticeable change in energy stability levels was observed. Similarly when the boom motion was brought to stop at t$\approx$15, a sharp decrease in the stability occurred (side 4) which is the direct result of the inertial forces/moments produced.

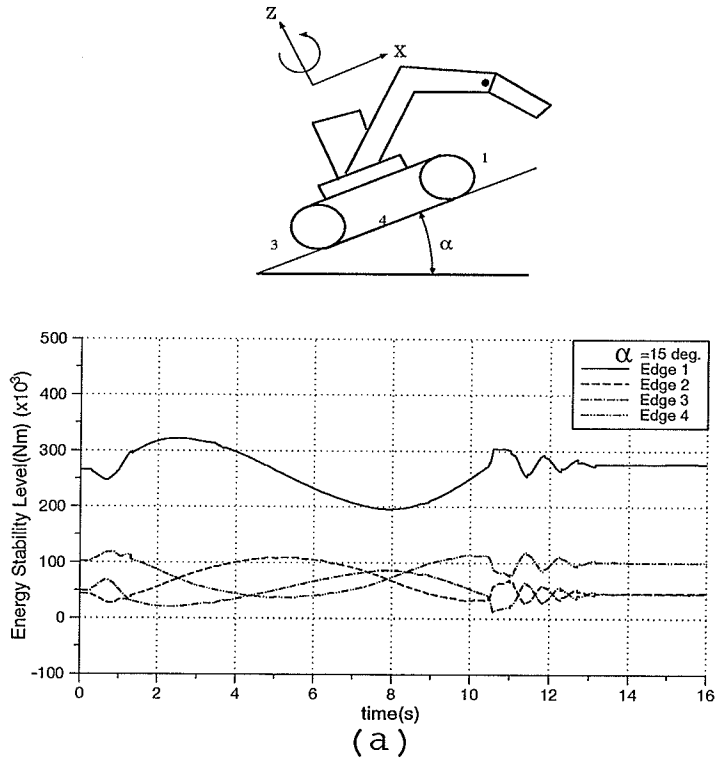

(a)

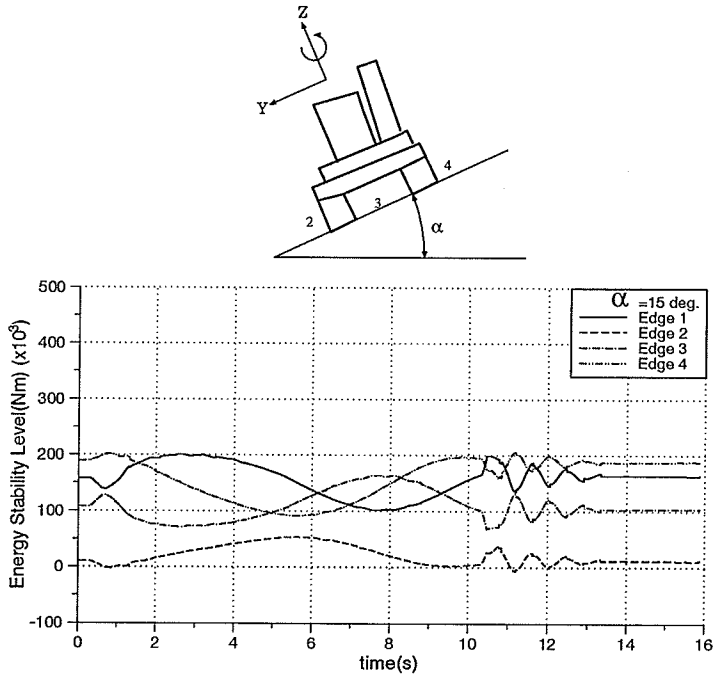

(b)

Figure 4.9: Effect of sloped ground.

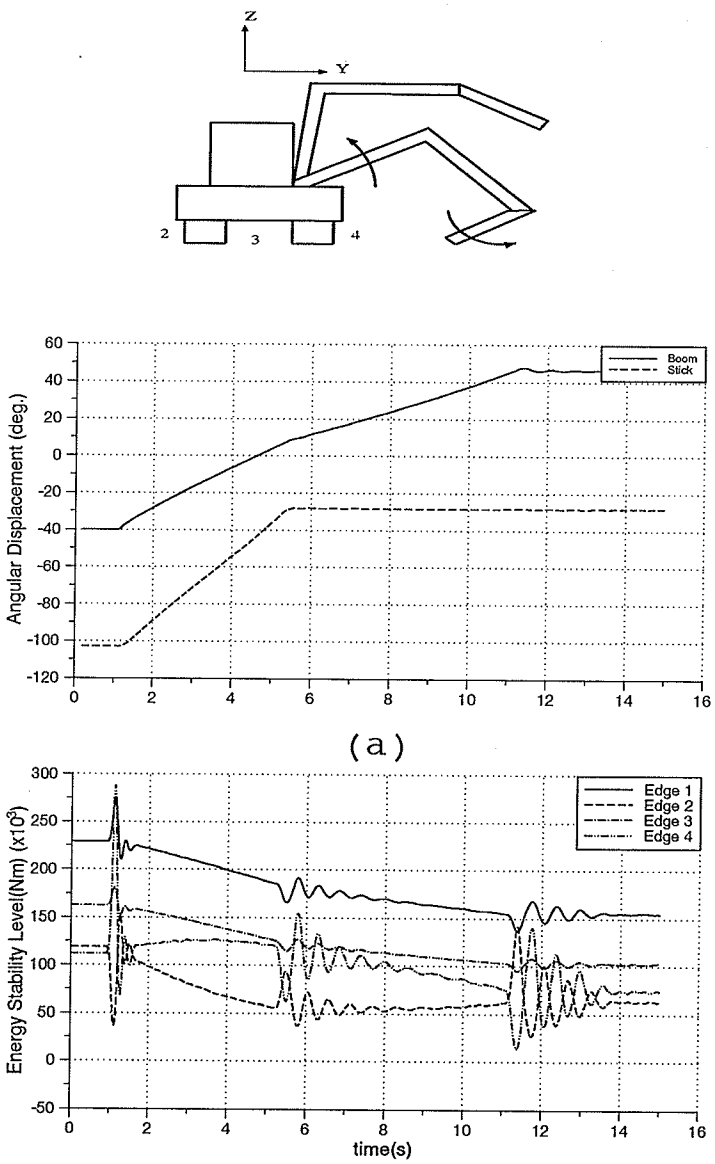

Figure 4.10: Effect of boom and stick motion.

4.2.8 Effect due to closed-loop interaction

Figure 4.11 shows a case when the machine, equipped with an excavation tool, performed a ditch digging operation. The force **F**, at the tool tip was modelled as a step function of time in the direction opposite to Z in the world coordinates. The velocity of the tool tip, **v**, was kept constant at 0.2 m/sec. Figure 4.11a shows the energy stability level changes during the operation. Figure 4.11b shows the effect of the external load by comparing the energy stability level with and without the external force. The external load as modelled here significantly reduced the energy stability level of edge 1.

4.2.9 Effect of support boundary change

Figure 4.12 shows a typical experiment designed to investigate the machine stability behavior when working in an unstructured environment. Here we simulate the situation when a rock is beneath one of the machine tracks while the machine is interacting with the environment (pushing against a wall for example). In such a case there are only three contact points with the ground and the support boundary is therefore a triangle. Figure 4.12 shows the energy stability level changes during the operation. External force is modelled as shown in the inset of Figure 4.12. This example represents a static case with no motion involved.

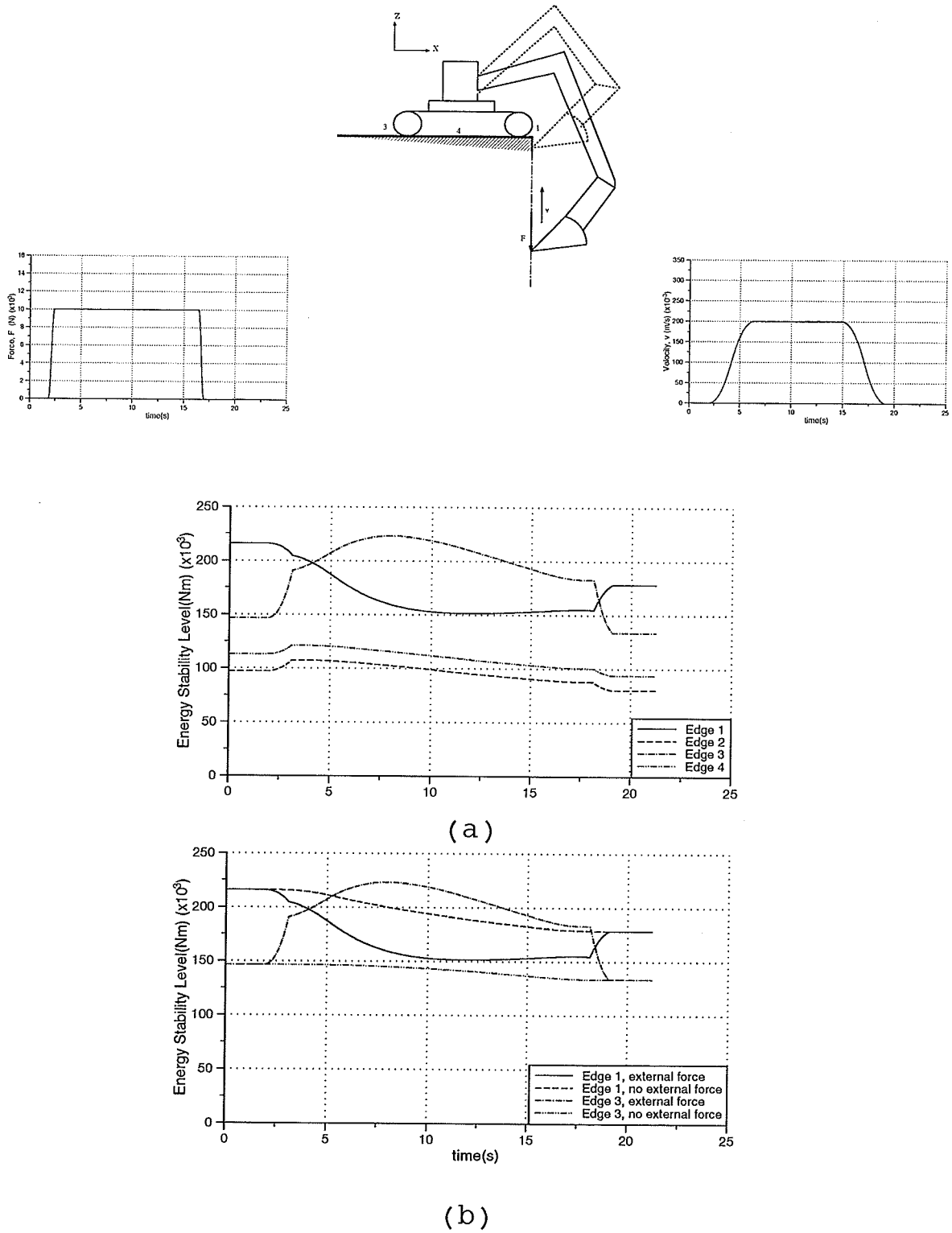

Figure 4.11: Effect of force interaction.

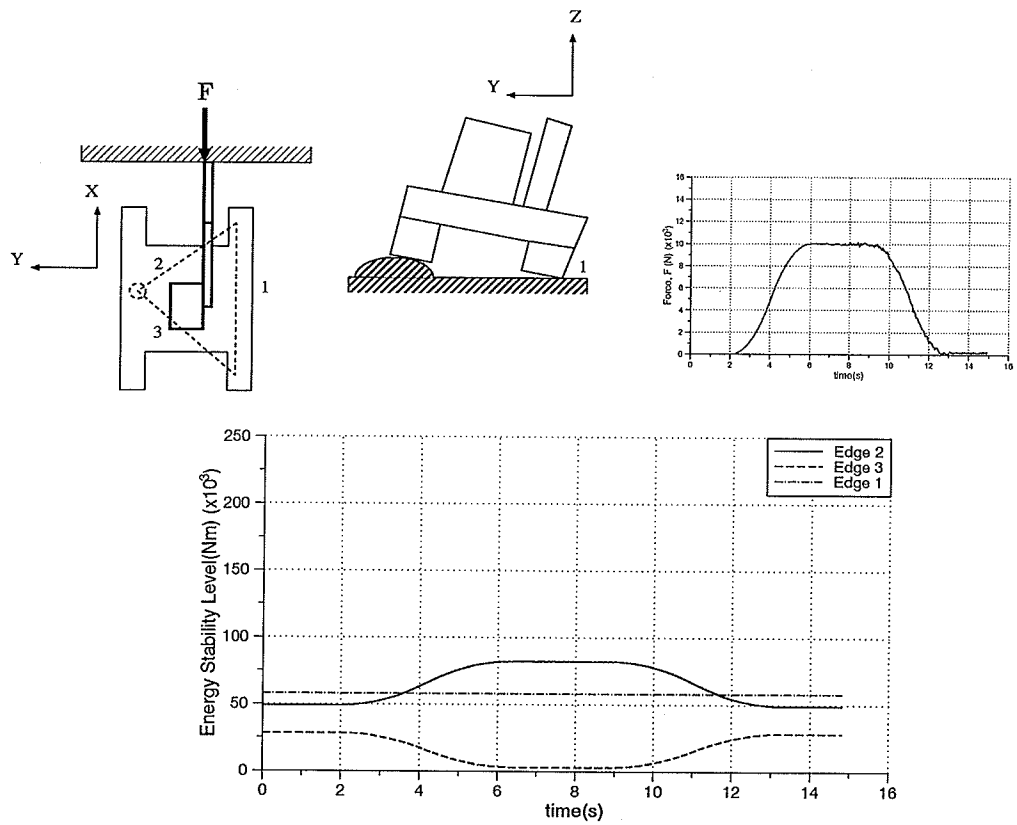

Figure 4.12: Three-sided support boundary.

Chapter 5

Graphical Display

The magnitude of energy stability levels for edges of the support boundary can be used towards providing a more efficient and hazard free operation of the machine. Ideally the information about energy stability levels can be used as input to a computer controlled system which limits the velocity and position of different joints so that the energy stability level is kept above a predetermined limit at all times. A rather simple alternative to the above approach for using the stability status information is to present this information in form of a graphical display. The objective in this chapter, is to find a suitable geometrical arrangement for the display. The display should be simple and able to convey as much information as possible regarding the stability condition of the machine.

5.1 Previous Work

Davidson and Schweitzer [6] suggested a graphical display based on their measure of stability, i.e., normalized virtual power (see Section 2.4). Figure 5.1 shows the display for a machine having four contact points with ground. Rectangle $ABCD$ which

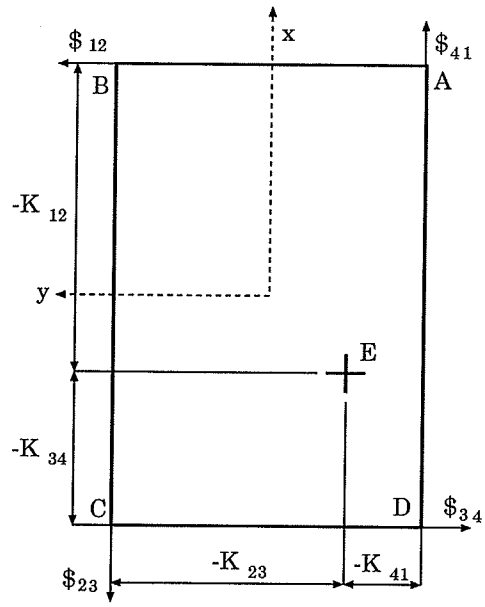

Figure 5.1: Graphical display arrangement from Davidson and Shweitzer [6].

represents the support boundary is formed using four normalized virtual powers, i.e., $K_{12}, K_{23}, K_{34}, K_{41}$. Point E, marks the position of the centre of gravity relative to machine frame xy. In this arrangement, the effect of changes in centre of gravity position is shown by the marker E and effect of external forces and moments are shown by changing the size of rectangle $ABCD$. Therefore the display has two changing elements; the centre of gravity and the boundary of the display. This might cause some problems in industrial applications [6].

Messuri and Klein [4] introduced a different display arrangement based on energy stability level. Figure 5.2 shows the display for a machine with five contact points with ground. The polygon $ABCDE$ is formed by horizontal projection of the support boundary. The marker F, shows the projection of the centre of gravity location on the horizontal plane. The dotted lines at each side of the polygon show the energy stability level for that side and therefore the hazard of tipping over. Note that this display has been primarily developed for walking machine applications. In these

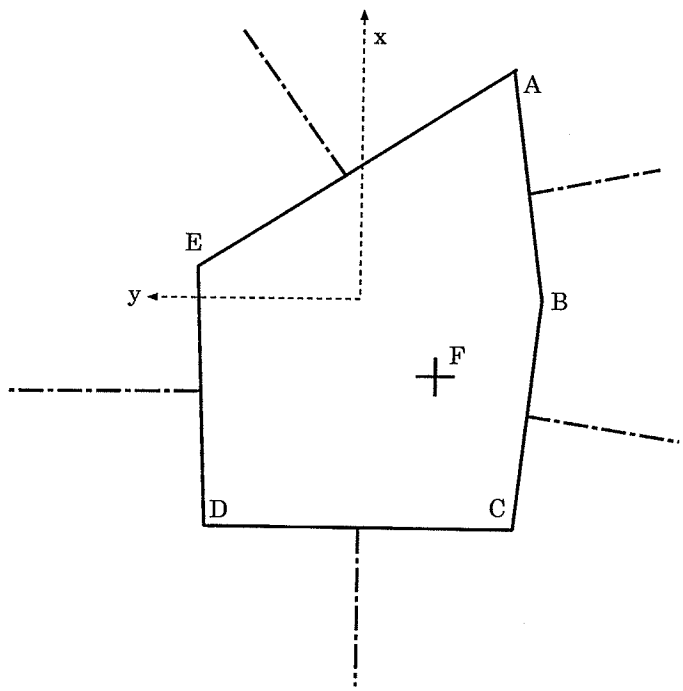

Figure 5.2: Graphical display arrangement from Messuri and Klein [4].

applications the motions and therefore changes in energy stability level are usualy slow and the complexity of the display is not a problem [4].

5.2 Display Arrangement

In this section a graphical display arrangement is proposed which suits the measure of stability developed in this thesis. The display has essentially two components. The first component is the display boundary. It simply shows the projection of the support boundary polygon onto the plane which coincides with the floor of the machine's cabin (i.e., parallel to **XY** plane of the machine frame **XYZ** in Figure 3.4). This means that the graphical representation of the support boundary will not change even when the machine is working on a sloping ground. The effect of sloping ground and/or spatially placed feet can be shown using another component of the graphical display

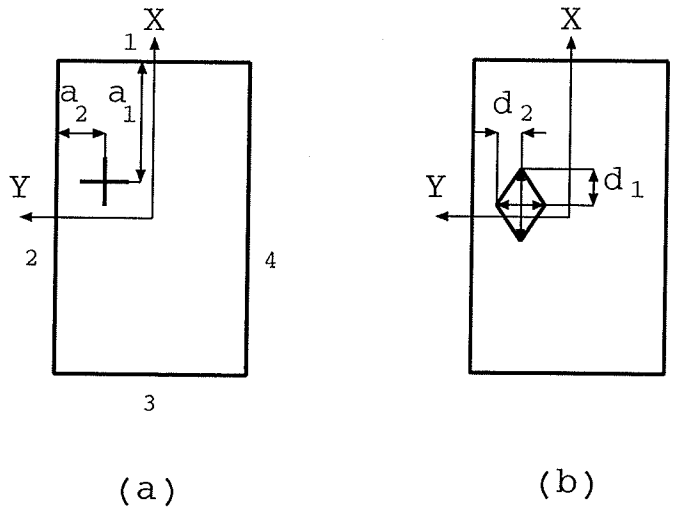

Figure 5.3: Stability marker polygon.

to be discussed in the next paragraph.

The second component of the graphical display is a marker indicating the current energy stability levels for all support boundary edges. The extended measure of stability defined in this thesis assigns a different value of energy stability level for each edge of the support boundary depending on the inertial/external loadings, deviation of the machine base from a level position etc. To convey all this information we introduce the concept of "stability marker polygon". Figure 5.3 shows how the stability marker polygon for a four sided support boundary is constructed. The polygon has the same number of sides as of the support boundary. When the machine is operating on a level ground and in the absence of inertial or external loads, the stability of the machine is determined by the position of the centre of gravity. In this case the stability marker polygon is reduced to a point, showing the projection of the centre of gravity on the display boundary. If other destabilizing loads appear or if the machine is on a sloping ground, a polygon is formed. Let E_1 be defined as the energy stability level of one side of the support boundary computed according to definitions presented in this thesis,

and E_2 be the energy stability level of the same side, if the machine was operating on a level ground with no destabilizing load other than its weight. The length, d_i, of each diagonal of the polygon facing the respective side of the support boundary is obtained from the following relations:

$$\Delta_i = (\frac{E_1}{E_2})_i \tag{5.1}$$

$$d_i = \begin{cases} (1 - \Delta_i)a_i & \Delta_i \leq 1 \\ 0 & \Delta_i > 1 \end{cases} \tag{5.2}$$

where i is the number of sides of the support boundary and a_i is the distance between each side of the support boundary and the centre of gravity (see Figure 5.3). Note that d_i is zero when the load is such that it helps the stability of the corresponding side of the support boundary. This will act as a factor of safety and at the same time helps the display to be less confusing.

Example 1. Figure 5.4 compares the display when machine is standing on level ground (Figure 5.4a) with the case when it is standing over a sloping ground (Figure 5.4b). The shape of the stability marker polygon reflects the lower energy stability level for the side 3 of the support boundary caused by the slope. Note that in both cases the display boundary remains the same.

Example 2. Figure 5.5 shows how the stability marker polygon reflects the effect of forces and moments arising from moving the arm. The example is taken from Section 4.2.7 (Figure 4.10) in which the boom and stick are moving upward. The figure shows the display at different instants. At t=0.05 the manipulator is stationary; at t=4.0 inertial loading is insignificant (constant velocity) therefore, the display only shows the position of the centre of gravity. At other instants shown in Figure 5.5 large inertial forces/moments are in effect, forming the stability marker polygon.

One of the advantages of the graphical display developed here is that the boundary of the display does not change and all the changes in the stability levels are reflected

on the stability marker polygon. Note also that because of the form of mapping used here to construct the stability marker polygon, the d_i does not have the same scale. In other words if the stability marker polygon is in the same distance from two sides of the support boundary, it does not necessarily mean that the energy stability level is the same for those sides.

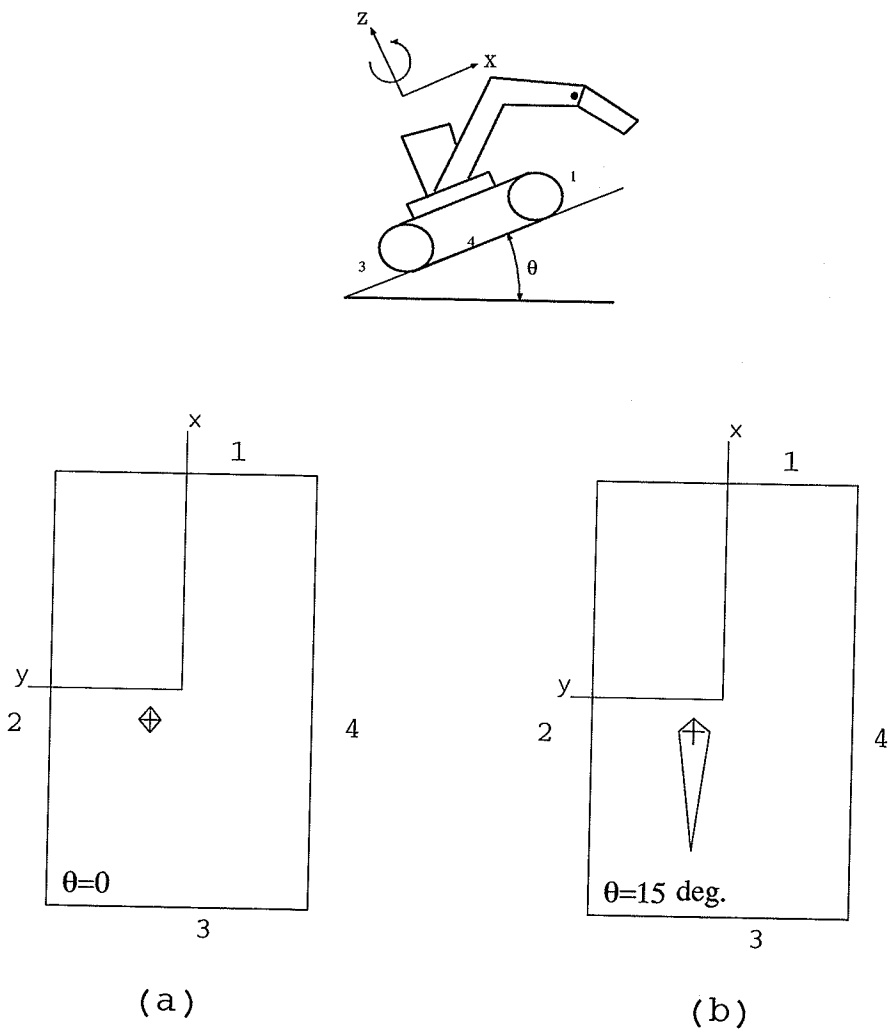

Figure 5.4: Effect of sloped ground on display; (a) machine on level ground; (b) machine on a slope.

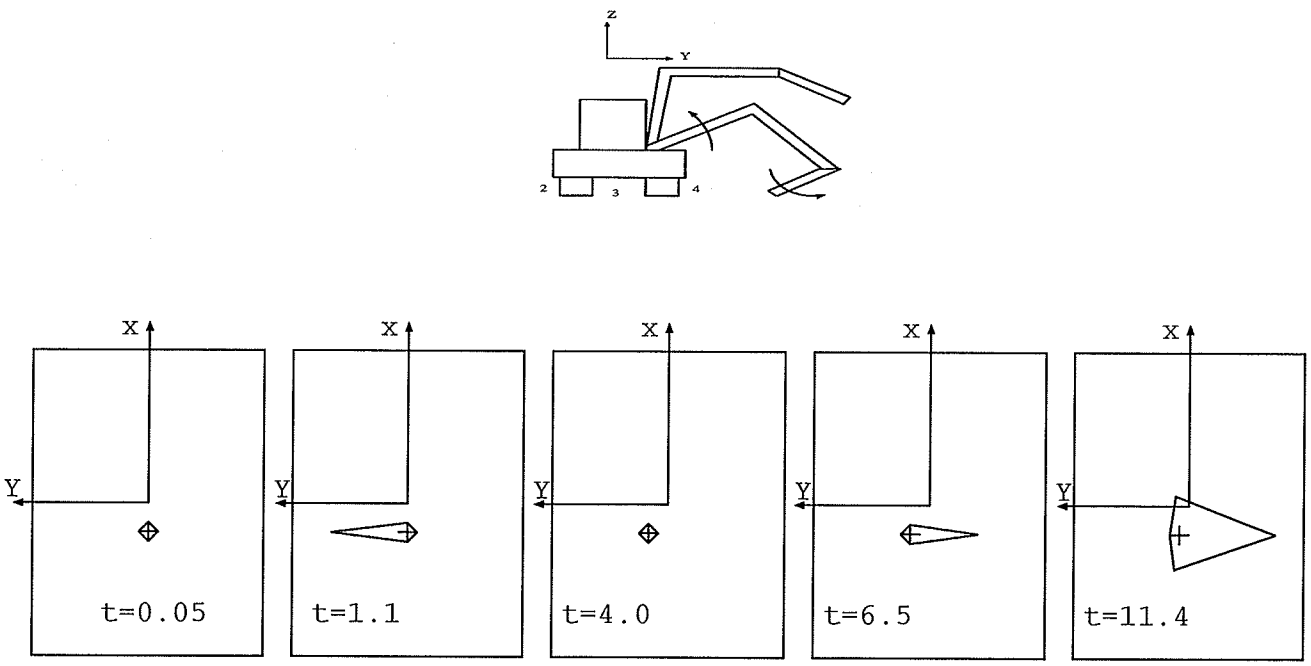

Figure 5.5: Effect of inertial loading on display (based on the result of Figure 4.10).

Chapter 6

Conclusions

6.1 Contributions of This Thesis

In this thesis a model which quantifies stability limits for a class of moving base manipulators was developed. The method is specially suited for applications where large forces and moments exist due to the interaction of the manipulator with the environment. The concept of energy stability level defined by Messuri and Klein [4] was extended here to include the effect of external and inertial forces/moments originating from the manipulator. Compared with the previously developed method by Davidson and Schweitzer [6], this new method can reflect the effect of *all factors* contributing to the stability condition including, spatially placed contact points with ground, rough terrain and top-heaviness.

The new model was then integrated within the simulator developed previously, in order to examine the stability characteristics of a candidate machine – an excavator-based log loader. The algorithm reflected the effect of forces/moments, arising from the manipulation of the implement, on the stability of the machine. While performing pick and placing tasks, the inertial forces and moments produced by moving the

manipulator arms had a significant effect on the stability of the machine. These effects were more pronounced during start and stop of the motion. It was also found that the action of the relief valves in the hydraulic system can influence the stability characteristics of the machine. By limiting the maximum pressure in the hydraulic system, a relief valve limits the inertial forces and moments. For a machine handling massive loads, this means that the larger the mass, the less will be the importance of the inertial loading on the stability. In other words, the stability of the machine depends primarily on the location of the centre of gravity (static stability). Furthermore, when carrying a load with considerable inertia, the orientation of grabbing the load was found to have a pronounced effect on the machine stability.

The average running time of the algorithm on a *Spark 2 Sun* workstation was $0.0167s$. This included the time spent for computation of the reaction forces and moments at the manipulator base which took $\approx 0.0148s$ of the total running time.

When the manipulator interacts with the environment in a closed-loop fashion, two cases could happen. First case is when it performs tasks such as scraping a surface, where the operation can be modeled as action of external forces/moments applied at the implement. In this case the effect of external forces/moments on stability assessment is reflected in the same way that the effect of inertial loads are considered. The second case is when the manipulator is used as a leg to form an additional support. In this case force interactions between the tool tip and ground is considered internal and should not be considered in the stability analysis.

A simple graphical display was also introduced for quantitatively displaying the stability condition of the machine. The new display is advantageous over other existing displays in that, the boundary of the display remains unchanged for the class of machines under investigation, and all the changes in the stability level are reflected on the stability polygon inside the display . The display which can be used for training or evaluation purposes is simple and can visually provide the human operator with

essential information regarding the stability conditions of the machine. The feasibility of applying the new display as compared to previously developed ones is, however, subject to future studies.

6.2 Suggestions for Future Work

The results of this work, which is believed to be a further contribution to the stability study of moving base manipulators, in general, and stability of heavy-duty machines in particular, can be included as part of a fault diagnostic system to relieve the operator from often non-intuitive and exhaustive task of maintaining the stability of the machine particularly in the presence of large external and inertial loadings. Ideally the information about energy stability levels can be used as input to a computer controlled system which senses an imminent upset, limits the velocity and position of different joints or even identifies correcting maneuvers and allowable payloads, so that the energy stability level is kept above a comfortable limit at all times. For example, if a loader is working on a slope and the computerized systems calculates that moving a particular log as instructed would result in overturning the vehicle, the system would advise the operator of the hazard in time for corrective action, thereby increasing job safety.

During the simulation study, it was observed that stopping the manipulator while in motion, can generate large inertial loading which negatively affect the stability of the machine. These inertial loads are generated instantly and if the loading is large enough to topple the machine, operator can do nothing to prevent it. It is therefore necessary to be able to predict the trend of changes in the stability of the machine. One method is to prepare a table with each entry containing a complete set of variables defining the state of the machine (positions, velocities, accelerations, inclinations, loads, etc.) and the margin of stability which would result if the machine was brought

to a sudden stop. The table can be constructed using a simulation program running off-line. Therefore at each instant a table look-up algorithm can find the margin of stability resulting from the effect of maximum possible inertia loading. Instead of the look-up table, a learning system, for example an Artificial Neural Network (ANN), can be trained to learn the relationship between the machine states and the margin of stability resulting from a sudden stop. The ability to generalize for unlearned cases and high processing speeds make the use of ANN attractive. The practicality of this approach however, requires further research.

References

[1] **Courteau, J.,** 1993, "Robotics in Canadian forestry", *IEEE Canadian review*, pp. 10-13.

[2] **McGhee, R. B.,** and **Frank, A. A.,** 1968, "On the Stability Properties of Quadruped Creeping Gait", *Mathematical Biosciences*, Vol. 3, No. 2, pp. 331-351.

[3] **Song, S.M.,** and **Waldron, K. J.,** 1987, "An Analytical Approach for Gait Study and Its Application on Wave Gaits", *The International Journal of Robotics Research*, Vol. 6, No. 2, pp 60-71.

[4] **Messuri, D.,** and **Klein, C. A.,** 1985, "Automatic Body Regulation for Maintaining Stability of a Legged Vehicle During Rough-Terrain Locomotion ", *IEEE J. Robotics and Automation*, Vol. RA-1, No. 3, pp. 132-141.

[5] **Wettergreen, D.,** and **Thrope, C.,** 1992, "Gait Generation for Legged Robots", *Proceedings 1992 IEEE/RSJ International Conference on Intelligent Robots and Systems*, pp. 1413-1420.

[6] **Davidson, J. K.,** and **Schweitzer, G.,** 1990, "A Mechanics-Based computer algorithm for Displaying the Margin of Static Stability in Four-Legged Vehicles", *ASME J. Mechanical Design*, Vol. 112, pp. 480-487.

[7] **Song, S.M.,** and **Waldron, K. J.,** 1989 , "Machines that Walk", MIT press.

[8] **Huang, M. Z.,** and **Waldron, K. J.,** 1990, "Relationship Between Payload and Speed in Legged Locomotion Systems", *IEEE Transactions On Robotics and Automation*, Vol. 6, No. 5, pp. 570-577.

[9] **Choi, B. S.,** and **Song, S. M.,** 1988, "Fully Automated Obstacle-Crossing Gaits for Walking Machines", *IEEE Transactions on Systems, Man and Cybernetics*, Vol. 18, No. 6, pp. 952-964

[10] **Qian, J.,** and **Gan, D.,** 1990, "Stability Study for Six-Legged Laterally-Walking Robots", *ASME, Design Engineering Division*, DE V15-3 PT3, New York, NY, pp. 171-176.

[11] **Hunt, K. H.**, 1978, *Kinematic Geometry of Mechanisms*, Clarendon Press, Oxford.

[12] **Lin, B. S.,** and **Song, S.M.,** 1993, "Dynamic Modeling, Stability and Energy Efficiency of A Quadrupedal Walking Machine", *IEEE International Conference on Robotics and Automation*, Vol. 3, pp. 367-373.

[13] **Paul, R. P.**, 1981, *Robot Manipulators: Mathematics, Programming and Control*, MIT Press, pp. 41-84.

[14] **Gardner, K. L.**, 1969, *A Programmed Vector Algebra*, Oxford University Press, pp. 194-205.

[15] **Lee, C. S. G.**, **Gonzalez, R. C.**, and **Fu, K. S.**, 1983, *Tutorial on Robotics*, Silver Spring, MD: IEEE Computer Society Papers.

[16] **Luh, J. Y. S., Walker , M. W.,** and **Paul, R. P. C.,** 1980, "On-line computational scheme for mechanical manipulators", *Journal of Dynamic Systems, Measurement, and Control*, Vol. 102, pp. 69-76.

[17] **Sepehri, N., Sassani, F.,** and **Lawrence, P.D.,** 1991, "Partitioned Hierarchical Modelling of Hydraulic Systems", *IASTED International Conference on Modelling and Simulation*, Calgary, Canada, pp. 170–174.

[18] **Sepehri, N., Lawrence, P.D., Sassani, F.,** and **Frenette, R.,** 1994, "Resolved-Mode Teleoperated Control of Heavy-Duty Hydraulic Machines", *ASME Journal of Dynamic Systems, Measurements and Control*, pp. 232–240.

[19] **Franklin D. Yealpe**, 1966, "Hydraulic and Pneumatic Power and Control", *McGraw-Hill,*.

[20] **Craig, J. J.**, 1989, *Introductions to Robotics*, Addison-Wesley Publishing Inc.

[21] **Lipkin, H.,** and **Duffy, J.,** 1982, "Analysis of Industrial Robots via the Theory of Screws", *Proc. of the 12th International Symposium on Industrial Robots*, Paris, France, June, pp. 359-370.

[22] **Bowns, D.E., Tomlinson, S.P.** and **Hull, S.R.**, 1983, "The Development of an Automatic Structured for Hydraulic System Design", *Proc. 39th Annual National Conf. on Fluid Power* Illinois, Vol. 37, pp. 302-309.

[23] **Cardona, A.** and **Geradin, M.**, 1990, "Modeling of a Hydraulic actuator in flexible Machine Dynamics Simulation", *Mech. Mach. Theory,* Vol. 25, No. 2, pp. 193-207.

[24] **Caney, K.**, 1970, "Integration Across Discontinuities in Ordinary Differential Equations Using Gear's Method", *University of Bath, School of Engineering, Report No. 478*, October 1970.

[25] **Gear, C.W.**, 1971, "Simultaneous Numerical Solution of Differential Algebraic Equations", *IEEE Trans. on Circuit Theory*, Vol. CT-18, No. 1, pp. 89-95.

[26] **Gear, C.W.**, 1972, "Numerical Initial Value Problem In Ordinary Differential Equations", *Prentice Hall.*

[27] **Bowns, D.E., Tomlinson, S.P.** and **Dorey, R.E.**, 1986, "Computer Simulation Techniques for The Dynamics Assessment of Fluid Power Systems", *7th Int. Fluid Power Symposium,* pp. 81-87.

Appendix A

Introduction to Screw Theory

There are two classes of vector quantities–free vectors and line vectors [20]. A free vector is specified by its magnitude and its direction and can be positioned anywhere in space without loss or change of its meaning. Examples of free vectors are vectors representing relative translational displacements (see Figure A.1a) or pure moments. A line vector refers to a vector whose effect, in addition to its direction and magnitude, is also dependent on its line of action. Examples of line vectors are those representing angular displacements (see Figure A.1b) or forces. Note that a unit vector is all that is necessary to specify a free vector while a line vector needs an additional specification which will be defined in the following.

The distinction between free and line vectors can be made by using the six plucker line coordinates [21]. Referring to Figure A.2, a line such as A can be uniquely described using the six Pluker line coordinates. The first three elements of the coordinates are the components of a unit vector $\tilde{\mathbf{a}}$ coaxial to the line whilst the next three elements are the components of the moment of the line about the origin o, i.e., $\vec{\mathbf{r}} \times \tilde{\mathbf{a}}$ [11]. $\vec{\mathbf{r}}$ is a vector extended from origin o to the line A. The unit line vector $\bar{A}$

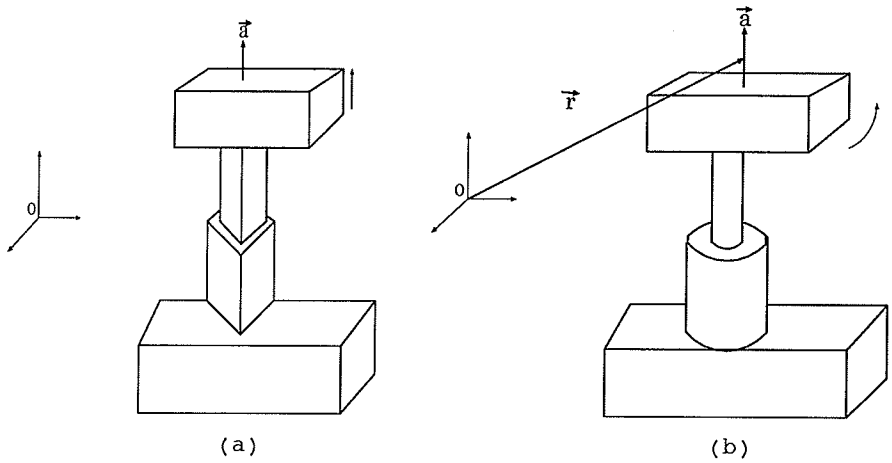

Figure A.1: Distinction between (a) a free vector and (b) a line vector [21]

associated with line A is then defined as,

$$\bar{A} = [\tilde{\mathbf{a}}; \vec{\mathbf{r}} \times \tilde{\mathbf{a}}] = [L, M, N; P, Q, R] \tag{A.1}$$

which is defined as a *unit* line vector. The six components constitute only four independent parameters as they are related by the following relations:

$$\tilde{\mathbf{a}} \cdot \tilde{\mathbf{a}} = 1$$

and

$$\tilde{\mathbf{a}} \cdot (\vec{\mathbf{r}} \times \tilde{\mathbf{a}}) = 0$$

Plucker coordinates of a line which connects point $[x_1, y_1, z_1, w_1]^T$ to point $[x_2, y_2, z_2, w_1]^T$

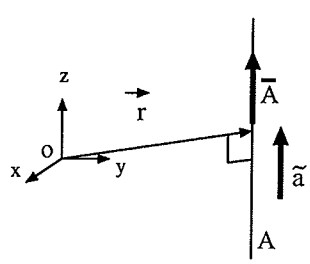

Figure A.2: The coordinates of a line in space

is obtained from the matrix

$$\begin{bmatrix} w_1 & x_1 & y_1 & z_1 \\ w_2 & x_2 & y_2 & z_2 \end{bmatrix} \tag{A.2}$$

where w_1 and w_2 are the homogeneous coordinates, usually taken to be unity. When each column is struck out in turn, the six plucker line coordinates are obtained as six determinants which are [11]:

$$L = \begin{vmatrix} w_1 & x_1 \\ w_2 & x_2 \end{vmatrix}, M = \begin{vmatrix} w_1 & y_1 \\ w_2 & y_2 \end{vmatrix}, N = \begin{vmatrix} w_1 & z_1 \\ w_2 & z_2 \end{vmatrix}$$

$$P = \begin{vmatrix} y_1 & z_1 \\ y_2 & z_2 \end{vmatrix}, Q = \begin{vmatrix} z_1 & x_1 \\ z_2 & x_2 \end{vmatrix}, R = \begin{vmatrix} x_1 & y_1 \\ x_2 & y_2 \end{vmatrix}$$

Now consider a force $\vec{F}$ which acts along a line with direction $\tilde{\mathbf{a}}$ (see Figure A3). The moment of the force about origin o is given by $|\vec{F}|(\vec{\mathbf{r}} \times \tilde{\mathbf{a}})$. The force can thus be expressed as a scalar multiple of a unit line vector $|\vec{F}|[\tilde{\mathbf{a}}; \vec{\mathbf{r}} \times \tilde{\mathbf{a}}]$.

The resultant of two general forces, $|\vec{F_1}|[\tilde{\mathbf{a}}_1; \vec{\mathbf{r}}_1 \times \tilde{\mathbf{a}}_1]$ and $|\vec{F_2}|[\tilde{\mathbf{a}}_2; \vec{\mathbf{r}}_2 \times \tilde{\mathbf{a}}_2]$ acting on a rigid body can be expressed by

$$|\vec{\mathbf{F}}|[\tilde{\mathbf{a}}_F; \vec{\mathbf{a}}_{o_F}] = [\vec{F_1} + \vec{F_2}; (\vec{\mathbf{r}}_1 \times \vec{F_1}) + (\vec{\mathbf{r}}_2 \times \vec{F_2})] \tag{A.3}$$

where $|\vec{\mathbf{F}}| = |\vec{F_1}| + |\vec{F_2}|$. Generally the resultant is not a pure force. If we decompose $\vec{\mathbf{a}}_{o_F}$ to components parallel and orthogonal to $\tilde{\mathbf{a}}$, the left hand side of the Equation

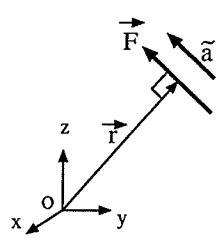

Figure A.3: Representation of a force using plucker line coordinates

(A.3) can be rewritten as [21]

$$|\vec{\mathbf{F}}|[\tilde{\mathbf{a}}_F; \vec{\mathbf{a}}_{o_F}] = |\vec{\mathbf{F}}|[\tilde{\mathbf{a}}_F; \vec{\mathbf{a}}_{o_F} - h\tilde{\mathbf{a}}_F] + |\vec{\mathbf{F}}|[\tilde{\mathbf{0}}; h\tilde{\mathbf{a}}_F] \tag{A.4}$$

where $h = (\tilde{\mathbf{a}_F} \cdot \vec{\mathbf{a}}_{o_F})/(\tilde{\mathbf{a}} \cdot \tilde{\mathbf{a}})$. $\tilde{\mathbf{0}}$ is the null vector. The first term on the right hand side of Equation (A.4) is a pure force while the second term is a moment parallel to the line of action of the force. This combination of force and moment is called a wrench with intensity $|\vec{\mathbf{F}}|$ and a pitch h. Note that for a pure force $h = 0$ and for a pure rotation $h = \infty$. Referring to discussion in Section 2.4, $[\tilde{\mathbf{a}}; \vec{\mathbf{r}} \times \tilde{\mathbf{a}}]$ represents the screw axis.

General motion of a rigid body consisting of rotation and translation can also be expressed using unit line vectors

$$|\vec{\omega}|[\tilde{\mathbf{a}}_\omega; \vec{\mathbf{a}}_{o_\omega}] \tag{A.5}$$

where $\vec{\omega}$ is the rigid body rotational velocity vector, $\vec{\mathbf{a}}_{o_\omega} = \vec{\mathbf{r}} \times \tilde{\mathbf{a}}_\omega$ and the pitch of the screw axis $h = (\tilde{\mathbf{a}}_\omega \cdot \vec{\mathbf{a}}_{o_\omega})/(\tilde{\mathbf{a}}_\omega \cdot \tilde{\mathbf{a}}_\omega)$. Here a pure rotation twist has a pitch of zero and a pure translation is represented by $h = \infty$ [21].

The instant power produced by a wrench $|\vec{\mathbf{F}}|[\tilde{\mathbf{a}}_F; \vec{\mathbf{a}}_{o_F}]$ acting on a rigid body which is constrained to twist about a screw, i.e. $|\vec{\omega}|[\tilde{\mathbf{a}}_\omega; \vec{\mathbf{a}}_{o_\omega}]$, is given by [21]

$$P = (\vec{\mathbf{F}} \cdot \vec{\mathbf{V}} + \vec{\omega} \cdot \vec{\mathbf{M}}) = |\vec{\mathbf{F}}||\vec{\omega}|(\vec{\mathbf{a}}_F \cdot \tilde{\mathbf{a}}_{o_\omega} + \tilde{\mathbf{a}}_\omega \cdot \vec{\mathbf{a}}_{o_F}) \tag{A.6}$$

For a rigid body in equilibrium $P = 0$, therefore,

$$|\vec{\mathbf{F}}||\vec{\omega}|(\vec{\mathbf{a}}_F \cdot \tilde{\mathbf{a}}_{o_\omega} + \tilde{\mathbf{a}}_\omega \cdot \vec{\mathbf{a}}_{o_F}) = 0 \tag{A.7}$$

Appendix B

215B Caterpillar Excavator Parameters

Figure B.1 shows the link frame attachment selected for the machine. The corresponding link parameters are shown in Table B.1. Transformation matrices for all the links of the machine are:

$$
{}^{0}A_1 = \begin{bmatrix} cos\theta_1 & 0 & sin\theta_1 & l_{11}cos\theta_1 \\ sin\theta_1 & 0 & -cos\theta_1 & l_{11}sin\theta_1 \\ 0 & 1 & 0 & 0 \\ 0 & 0 & 0 & 1 \end{bmatrix} \tag{B.1}
$$

$$
{}^{1}A_2 = \begin{bmatrix} cos\theta_2 & -sin\theta_2 & 0 & l_2cos\theta_2 \\ sin\theta_2 & cos\theta_2 & 0 & l_2sin\theta_2 \\ 0 & 0 & 1 & 0 \\ 0 & 0 & 0 & 1 \end{bmatrix} \tag{B.2}
$$

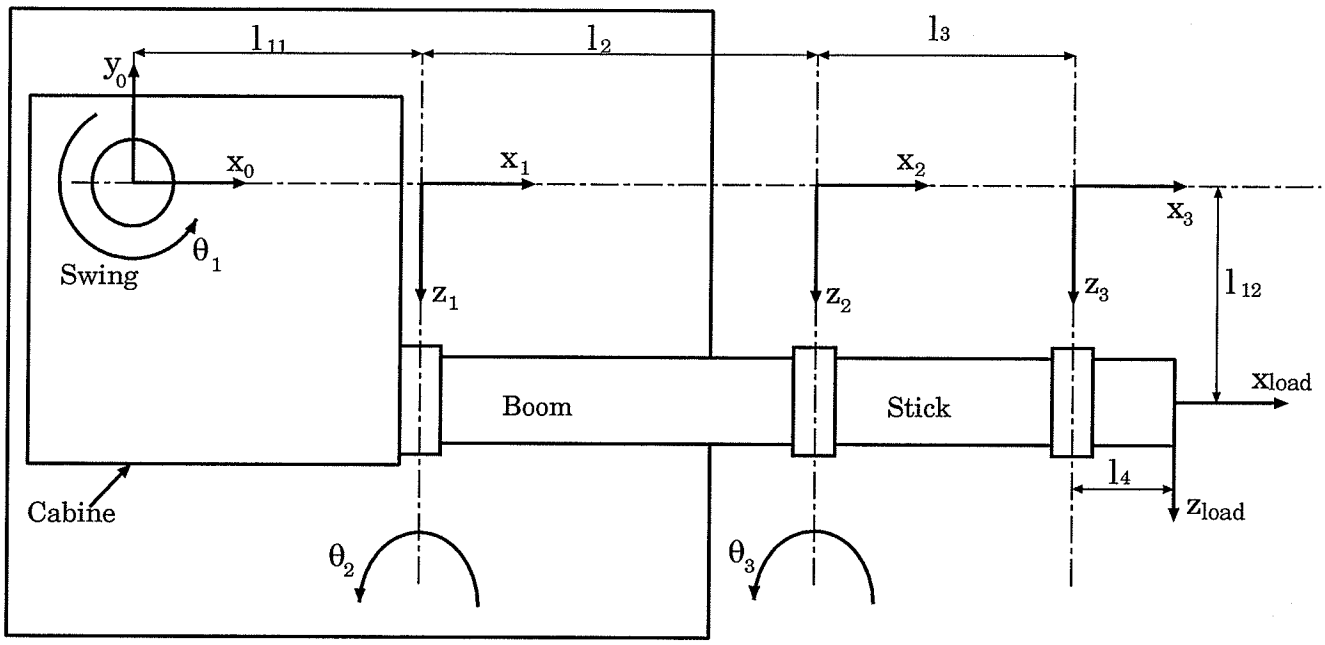

Figure B.1: Frame attach for links of the manipulator.

$$
{}^{2}A_3 = \begin{bmatrix} cos\theta_3 & -sin\theta_3 & 0 & l_3cos\theta_3 \\ sin\theta_3 & cos\theta_3 & 0 & l_3sin\theta_3 \\ 0 & 0 & 1 & 0 \\ 0 & 0 & 0 & 1 \end{bmatrix} \tag{B.3}
$$

${}^{4}A_{load}$ which is the homogeneous transformation between the load and the manipulator's last link frame is:

$$
{}^{4}A_{load} = \begin{bmatrix} 1 & 0 & 0 & l_4 \\ 0 & 1 & 0 & 0 \\ 0 & 0 & 1 & l_{12} \\ 0 & 0 & 0 & 1 \end{bmatrix} \tag{B.4}
$$

where $l_{12} = 0.12m$. Table B.2 shows the data for mass and location of the center of gravity for each link of the manipulator. Note that the location of the centre of gravity is given with respect to the frame attached to each link (see Figure B.1).

Table B.3 shows the components of the inertia tensor matrix (Equation B.5) for

each link of the manipulator. Note that the inertia tensor is also defined with respect to the frame attached to each link and therefore remains constant regardless of the position of the link relative to the machine frame [15].

$$
{}^{i}I_i = \begin{bmatrix} \frac{-I_{xx}+I_{yy}+I_{zz}}{2} + m_i\bar{x}_i^2 & I_{xy} & I_{xz} \\ I_{xy} & \frac{I_{xx}-I_{yy}+I_{zz}}{2} + m_i\bar{y}_i^2 & I_{yz} \\ I_{xz} & I_{yz} & \frac{I_{xx}+I_{yy}-I_{zz}}{2} + m_i\bar{z}_i^2 \end{bmatrix} \tag{B.5}
$$

Table B.1: Link parameters.

Joint	variable	$\theta_i(deg.)$	$\alpha_i(deg.)$	$a_i(m)$	$d_i(m)$
1	θ_1	0	90	$l_{11} = 0.35$	0
2	θ_2	0	0	$l_2 = 5.2$	0
3	θ_3	0	0	$l_3 = 1.8$	0

Table B.2: Mass and centre of gravity data.

link	m(kg)	$\bar{x}(m)$	$\bar{y}(m)$	$\bar{z}(m)$
Swing	8031	-1.4	0	-0.16
Boom	1830	-2.9	0.2	0
Stick	688	-0.9	0.1	0

Table B.3: Inertia tensor data.

link	$I_{xx}(kg\ m^2)$	$I_{yy}(kg\ m^2)$	$I_{zz}(kg\ m^2)$	$I_{xy}(kg\ m^2)$	$I_{xz}(kg\ m^2)$	$I_{yz}(kg\ m^2)$
Swing	15700	0	200	0	0	0
Boom	15400	100	0	-1100	0	0
Stick	600	10	0	0	-70	0

Appendix C

Contributions to the Simulation Model

C.1 Effect of a Non-level Base.

To include the effect of operation over a non-level ground on the stability of the machine, we needed to include the effect of a non-level base in the simulation model of the machine . Note that this is a modification in structure subsystem of the original model . The general dynamic equation of the manipulator derived by Lagrangian method is in the form:

$$F_i = \sum_{j=i}^{4} D_{ij}\ddot{\theta}_j + \sum_{j=i}^{4}\sum_{k=i}^{4} D_{ijk}\dot{\theta}_j\dot{\theta}_k + D_i \tag{C.1}$$

where F_{ij} is a generalized force, D_{ij} is the effective inertia matrix, D_{ijk} is the coefficient representing centripetal and Coriolis effects and D_i is the term related to the gravity loading. The only term in Equation (C.1) affected by a non-level manipulator base is the gravity term D_i which is computed from the following expression:

$$D_i = \sum_{p=i}^{4} m_p g^T \frac{\partial T_p}{\partial \theta_i} \hat{r}_p^p \tag{C.2}$$

where m_p is the mass, g is the column vector representation of the gravity vector $\vec{\mathbf{g}}$, T_p is the related homogeneous transformation of manipulator links and $\hat{r}_p^p$ is the position vector of the centre of gravity of the link in its own frame. To include the effect of inclination, we only need to modify $\vec{\mathbf{g}}$. In Section 3.1.2 we defined the base deviations from level position by attitudinal angles for roll and pitch of the machine frame **XYZ** with respect to the gravity frame $\bar{\mathbf{X}}\bar{\mathbf{Y}}\bar{\mathbf{Z}}$ (see Figure 3.5). The same rotational transformations are used to modify $\vec{\mathbf{g}}$ when the machine frame is in a non-level position, i.e.,

$$\vec{\mathbf{g}} = Rot(y, -\phi_y)Rot(x, -\phi_x)\begin{bmatrix} 0 \\ 0 \\ -g \end{bmatrix} \tag{C.3}$$

where $Rot(y, -\phi_y)$ and $Rot(x, -\phi_x)$ are rotation matrices defined as [13],

$$Rot(y, -\phi_y) = \begin{bmatrix} cos\phi_y & 0 & -sin\phi_y \\ 0 & 1 & 0 \\ sin\phi_y & 0 & cos\phi_y \end{bmatrix} \tag{C.4}$$

$$Rot(x, -\phi_x) = \begin{bmatrix} 1 & 0 & 0 \\ 0 & cos\phi_x & sin\phi_x \\ 0 & -sin\phi_x & cos\phi_x \end{bmatrix} \tag{C.5}$$

Therefore we have,

$$\vec{\mathbf{g}} = \begin{bmatrix} cos\phi_y & sin\phi_y sin\phi_x & -sin\phi_y cos\phi_x \\ 0 & cos\phi_x & sin\phi_x \\ sin\phi_y & -sin\phi_x cos\phi_y & cos\phi_y cos\phi_x \end{bmatrix}\begin{bmatrix} 0 \\ 0 \\ -g \end{bmatrix} = \begin{bmatrix} sin\phi_y cos\phi_x g \\ -sin\phi_x g \\ -cos\phi_y cos\phi_x g \end{bmatrix} \tag{C.6}$$

Note that $\vec{\mathbf{g}}$ is defined in **XYZ** frame. This modified $\vec{\mathbf{g}}$ is used in the dynamic model of the manipulator.

C.2 Modeling End-of-Stroke Condition.

The importance of dynamic analysis of fluid power systems has been recognized for a long time [22,23]. One of the discontinuous nonlinearities which occur in hydraulic systems is when the actuators encounter end stops and a significant dynamic shock force is generated (Figure C.1) [19]. As this kind of dynamic forces can affect the stability of a machine carrying a hydraulically actuated manipulator, it was essential to model this phenomenon.

To reduce the shock forces generated at the end of stroke, all hydraulic actuators are usually equipped with one or another kind of hydraulic dashpots. The main objective in using dashpots is to decelerate the piston with a controlled force, strong enough to reverse the stroke swiftly but not so fast that it shocks other operating components. Therefore to model the end-of-stroke condition, one should also model the dashpot effect. One method to model the end-of-stroke condition is to assume that the unit is brought to rest instantaneously. This simply implies stopping the integrator and performing a restart which is unattractive due to the penalty in computational effort [24]. Imposing a very high deceleration will make the system mathematically stiff. Although gear stiff method is capable of coping with this stiffness [25,26], it may involve significant computational effort. It is prudent to avoid stiffness at the modeling stage. The second method at bringing the actuator to rest at appropriate position involves reducing the driving force, increasing the viscous friction coefficient and the introduction of a spring rate into the equations [27].

Here we introduce a rather simple, yet effective, model which in concept is similar to the above approach but differs in implementation in that it maintains the actual force at its true value and does not require to artificially introduce a spring rate or damping into the model. In developing this model two important issues are considered; the capability of the model of being added to the existing simulation program

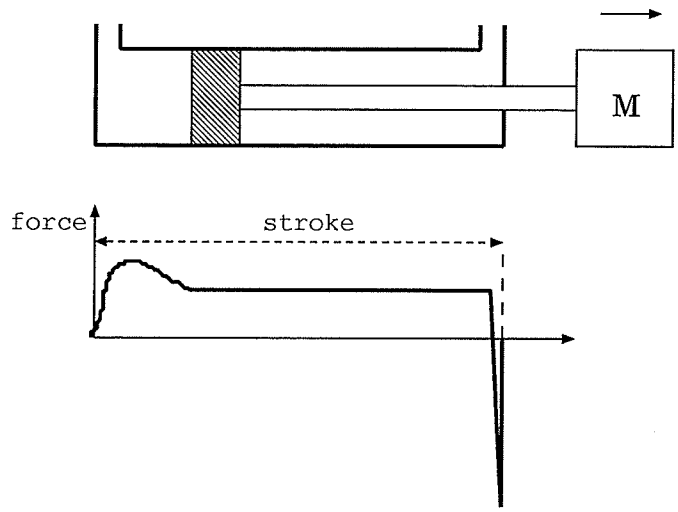

Figure C.1: Undamped hydraulic cylinder.

without disturbing the description of other component models and, its capability of allowing to employ large time steps without encouraging instability or divergence.

Referring to Figure C.2, when the piston reaches the end of stroke we have $P_1 = P_s$ and $P_2 = P_e$, where P_s is the maximum pressure allowed in the hydraulic line (set by a relief valve) and P_e is the return (tank) pressure. The manner in which the line pressures arrive at the above levels depends on the dashpot characteristics. Here we introduce a virtual pressure, P_{vir}, which should in fact resembles the back pressure in a dashpot. This pressure is activated at a distance δ from the end-of-stroke and is added to the line pressures (P_i or P_o depending on the direction of motion). The virtual pressure changes linearly with the stroke (see Figure C.3), i.e.,

$$P_{vir} = \begin{cases} P(1 - \frac{l_{lim}-l}{\delta}) & when \quad l_{lim} - l \leq \delta \\ 0 & when \quad l_{lim} - l > \delta \end{cases} \tag{C.7}$$

Here l is the piston displacement and l_{lim} is the end of stroke length. δ and P are the two parameters which are to be adjusted for different types of hydraulic cylinders and dashpots. P is normally chosen to be greater than the maximum pump pressure. It should be large enough to bring the piston to a stop even in the presence of load. δ, on

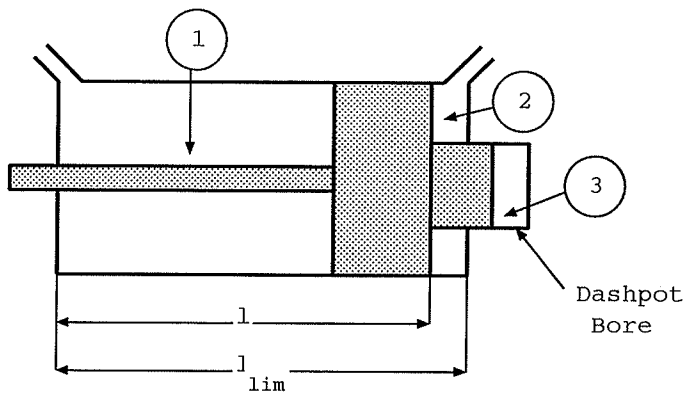

Figure C.2: Hydraulic cylinder near the end of stroke.

the other hand, is used to fine tune the expression for P_{vir} such that the decelerating characteristics of a specific dashpot is simulated properly.

To show the applicability of the above formulation for simulating the end-of-stroke condition in hydraulic manipulators, two cases were studied. The first case was the simulation of the up/down motion of link two of a Unimate MK-II hydraulic robot (Figure C.4). The second case was the simulation of the in/out motion of stick link of 215B Caterpillar Excavator (Figure 1.1).

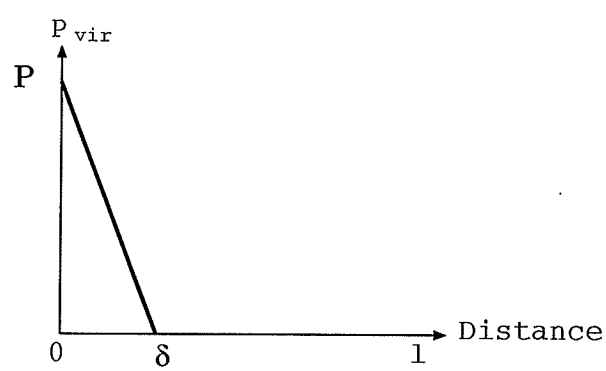

Figure C.3: Virtual pressure distribution.

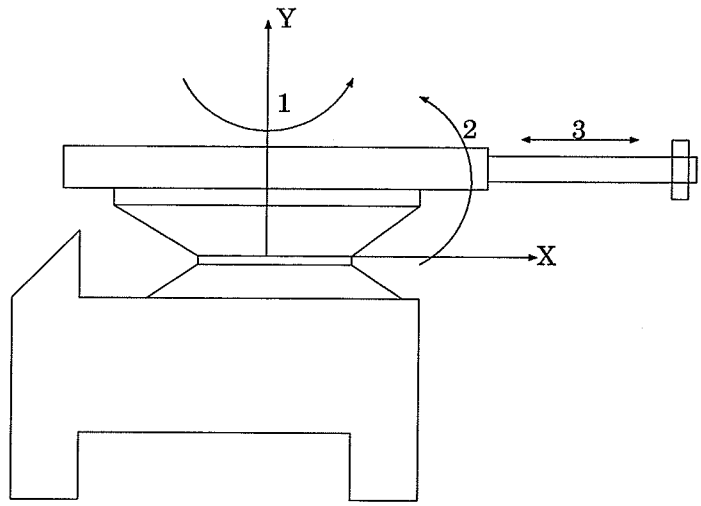

Figure C.4: Unimate MK-II robot.

Case One: Unimate MK-II Robot. The experimental results are shown in Figure C.5a where the measured joint angles and accelerations are plotted. The simulation results are shown in Figure c.5b. The simulation results are in agreement with the experiments. Figures C.6a and C.6b compare the pressure patterns. It is seen that once the joint limit is encountered, the input pressure rises to its limit while the output pressure drops to the atmospheric pressure.

Case Two: 215B Caterpillar Excavator. The second case, the stick was moved out until it was brought to stop by hitting its joint limit (see Figure C.7a). Again the end-of-stroke deceleration pattern was successfully simulated. The result is shown in Figure C.7b. Comparing with the experimental observation, the joint limit condition was simulated with reasonable accuracy. The changes in the acceleration observed in the experiments were due to the changes in the input voltage originated from the joystick controlled by the machine operator. In the simulation the input voltage to the stick main valve was kept constant. The inset in Figure C.7b shows the effect of varying the parameter δ in the simulation. A selected value of $\delta = 5\%$ gives an

acceptable result. A higher δ results in lower values for deceleration and a smaller δ produces a large deceleration effect. The simulated line pressures variations is also included in Figure C.7c which is similar to the pattern shown in Figs. C.6a and C.6b.

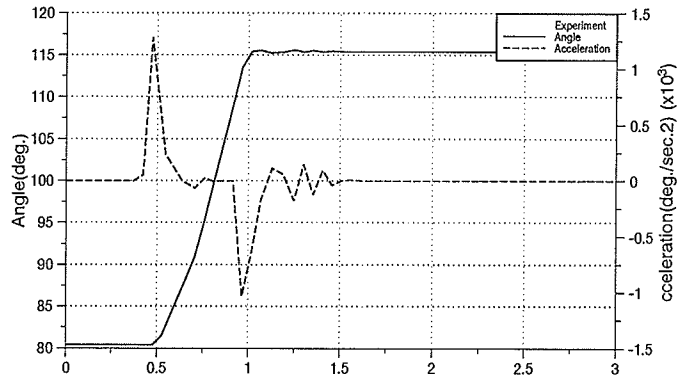

(a)

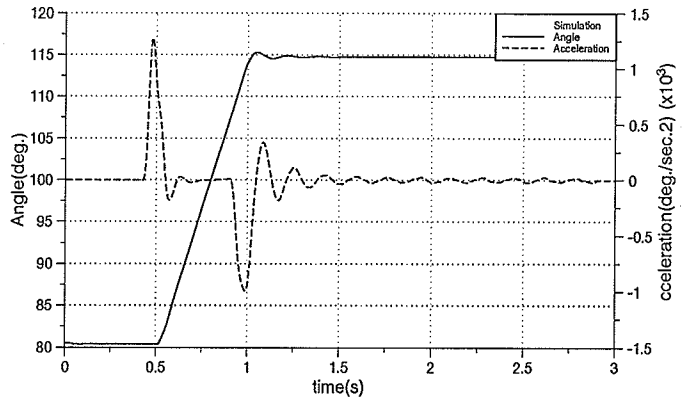

(b)

Figure C.5: (a) Unimate MK-II robot experimental result; (b) Simulation result.

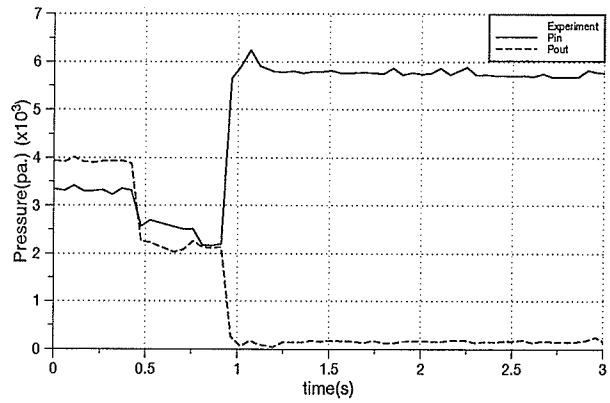

(a)

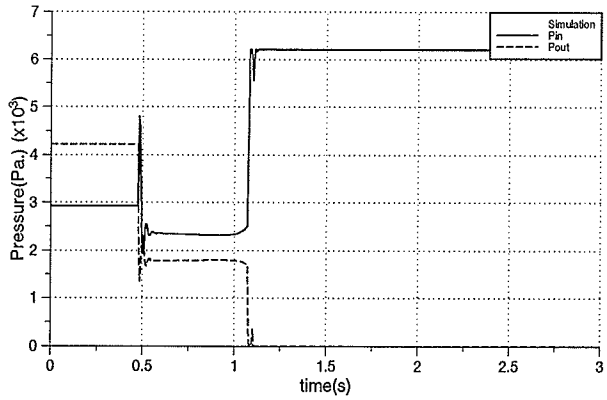

(b)

Figure C.6: Unimate MK-II robot pressure change; (a) Experiment, (b) Simulation.

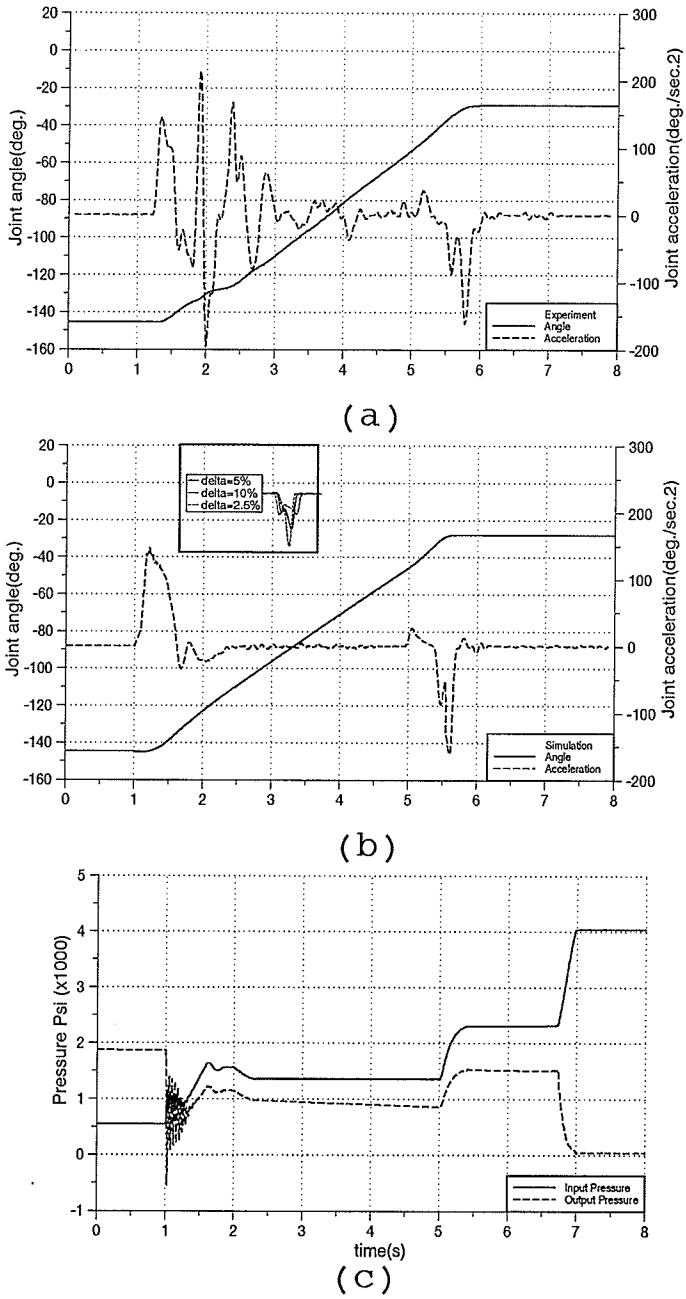

Figure C.7: (a) Excavator experimental results; (b) Excavator simulation results (c) Excavator pressure changes (Simulation).